

Andean Geology

ISSN: 0718-7092

revgeologica@sernageomin.cl

Servicio Nacional de Geología y Minería Chile

Bense, Frithjof; Costa, Carlos; Oriolo, Sebastián; Löbens, Stefan; Dunkl, István; Wemmer,
Klaus; Siegesmund, Siegfried
Exhumation history and landscape evolution of the Sierra de San Luis (Sierras
Pampeanas, Argentina) - new insights from low - temperature thermochronological data
Andean Geology, vol. 44, núm. 3, septiembre, 2017, pp. 275-306
Servicio Nacional de Geología y Minería
Santiago, Chile

Available in: http://www.redalyc.org/articulo.oa?id=173952866003



Complete issue

More information about this article

Journal's homepage in redalyc.org



Andean Geology 44 (3): 275-306. September, 2017

doi: 10.5027/andgeoV44n3-a03

## Exhumation history and landscape evolution of the Sierra de San Luis (Sierras Pampeanas, Argentina) - new insights from low temperature thermochronological data

Frithjof Bense<sup>1, 2</sup>, Carlos Costa<sup>3</sup>, Sebastián Oriolo<sup>1</sup>, Stefan Löbens<sup>1</sup>, István Dunkl<sup>1</sup>, Klaus Wemmer<sup>1</sup>, \*Siegfried Siegesmund<sup>1</sup>

- <sup>1</sup> Geoscience Centre, University of Göttingen, Goldschmidtstraße 3, 37077 Göttingen, Germany.

  seba.oriolo@gmail.com; stefan\_loebens@fels.de; istvan.dunkl@geo.uni-goettingen.de; kwemmer@gwdg.de; ssieges@gwdg.de
- <sup>2</sup> Federal Institute for Geosciences and Natural Resources, Stilleweg 2, 30655 Hannover, Germany. frithjof.bense@bgr.de
- <sup>3</sup> Departamento de Geología, Universidad Nacional de San Luis, Chacabuco 917, 5700 San Luis, Argentina. costa@unsl.edu.ar

ABSTRACT. This paper presents low-temperature thermochronological data and K-Ar fault gouge ages from the Sierra de San Luis in the Eastern Sierras Pampeanas in order to constrain its low-temperature thermal evolution and exhumation history. Thermal modelling based on (U-Th)/He dating of apatite and zircon and apatite fission track dating point to the Middle Permian and the Triassic/Early Jurassic as main cooling/exhumation phases, equivalent to *ca.* 40-50% of the total exhumation recorded by the applied methods. Cooling rates are generally low to moderate, varying between 2-10 °C/Ma during the Permian and Triassic periods and 0.5-1.5 °C/Ma in post-Triassic times. Slow cooling and, thus, persistent residence of samples in partial retention/partial annealing temperature conditions strongly influenced obtained ages. Thermochronological data indicate no significant exhumation after Cretaceous times, suggesting that sampled rocks were already at or near surface by the Cretaceous or even before. As consequence, Cenozoic cooling rates are low, generally between 0.2-0.5 °C/Ma which is, depending on geothermal gradient used for calculation, equivalent to a total Cenozoic exhumation of 0.6-1.8 km. K-Ar fault gouge data reveal long-term brittle fault activity. Fault gouge ages constrain the end of ductile and onset of brittle deformation in the Sierra de San Luis to the Late Carboniferous/Early Permian. Youngest K-Ar illite ages of 222-172 Ma are interpreted to represent the last illite formation event, although fault activity is recorded up to the Holocene.

Keywords: Sierras Pampeanas, Sierra de San Luis, K-Ar dating, Fault gouge, Illite dating, Polytype quantification, Thermochronology, Helium dating, Fission track.

RESUMEN. Historia de la exhumación y evolución del paisaje de la sierra de San Luis (Sierras Pampeanas, Argentina)-nuevas perspectivas a partir de datos termocronológicos de baja temperatura. Esta contribución presenta datos de termocronología de baja temperatura y edades de illitas generadas en zonas de fallas de la sierra de San Luis, en las Sierras Pampeanas Orientales de Argentina, con el propósito de aportar al conocimiento de la historia de su exhumación y evolución termal de baja temperatura. El modelado termal basado en dataciones de (U-Th)/He, apatita, circón y trazas de fisión sugiere que las principales fases de exhumación y enfriamiento ocurrieron durante el Pérmico medio y Triásico/Jurásico inferior, contribuyendo con aproximadamente 40-50% de la exhumación total registrada por los métodos utilizados. Las tasas de enfriamiento son, en general, bajas a moderadas, variando entre 2-10 °C/Ma durante el Pérmico y Triásico y 0,5-1,5 °C/Ma después del este último período. El lento enfriamiento y la persistente residencia de las muestras analizadas en condiciones térmicas de retención parcial (partial annealing) ha influenciado notoriamente las edades obtenidas. Los datos termocronológicos indican que no ha habido una exhumación

<sup>\*</sup> Corresponding author: ssieges@gwdg.de

significativa después del Cretácico o incluso antes. Consecuentemente, las tasas de enfriamiento durante el Cenozoico, son bajas, generalmente 0,2-0,5 °C/Ma, las cuales equivalen a una exhumación total para el Cenozoico de 0,6-1,8 km, según el gradiente geotérmico que se use para su cálculo. Las dataciones K-Ar en arcillas generadas en zonas de fallas han revelado el desarrollo deformación frágil en la Sierra de San Luis hasta el Carbonífero superior/Pérmico inferior. Las edades más jóvenes de illitas obtenidas por datación K-Ar de 222-172 Ma se interpreta que representan el último evento de formación de illita por deformación frágil en las muestras analizadas, aunque la actividad del fallamiento ha sido registrada hasta el Holoceno.

Palabras clave: Sierras Pampeanas, Sierra de San Luis, Datación K-Ar, Gouge de falla, Datación de illita, Cuantificación de politipos, Termocronología, Datación con helio, Trazas de fisión.

#### 1. Introduction

The Sierra de San Luis is one of the southernmost ranges of the Sierras Pampeanas region (Pampean ranges, Fig. 1). These ranges correspond to basement block uplifts surrounded by basins of flat topography, which widely crop out in central-western Argentina between 27° to 33°30' S (Ramos *et al.*, 2002 and references therein). This region is also regarded as an example of active thick-skinned

crustal deformation related to flattening of the Nazca plate subduction since ~15 Ma (Jordan *et al.*, 1983; Jordan and Allmendinger, 1986; Kay and Abbruzzi, 1996; Ramos *et al.*, 2002). Although the Sierras Pampeanas show a different and longer evolutionary paths than the Andean orogen, they share a similar morphogenetic history after the flattening of the Nazca plate and are regarded as a morphotectonic component of the Andean building (Jordan and Allmendinger, 1986).

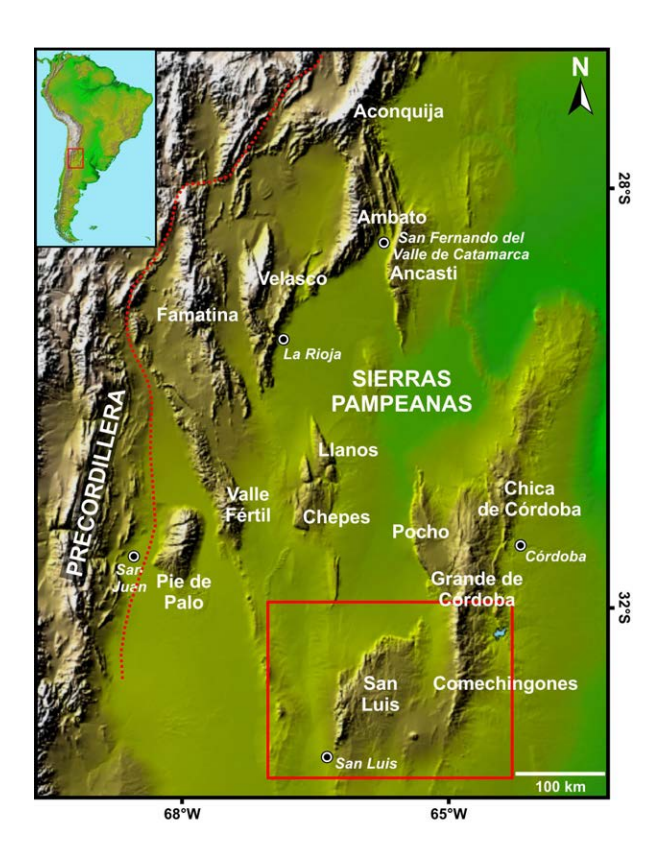


FIG. 1. Digital elevation model of the Sierras Pampeanas region where fault-bounded blocks surrounded by intermontane basins stand out in central western Argentina (see inset for location). Red dotted line shows boundaries of this geologic province with the main Andean building. Red rectangle highlights the Sierra de San Luis area depicted in figure 2 (NASA SRTM data http://www2.jpl.nasa.gov/srtm/southAmerica.htm#PIA03388) (last visit 01/09/2016).

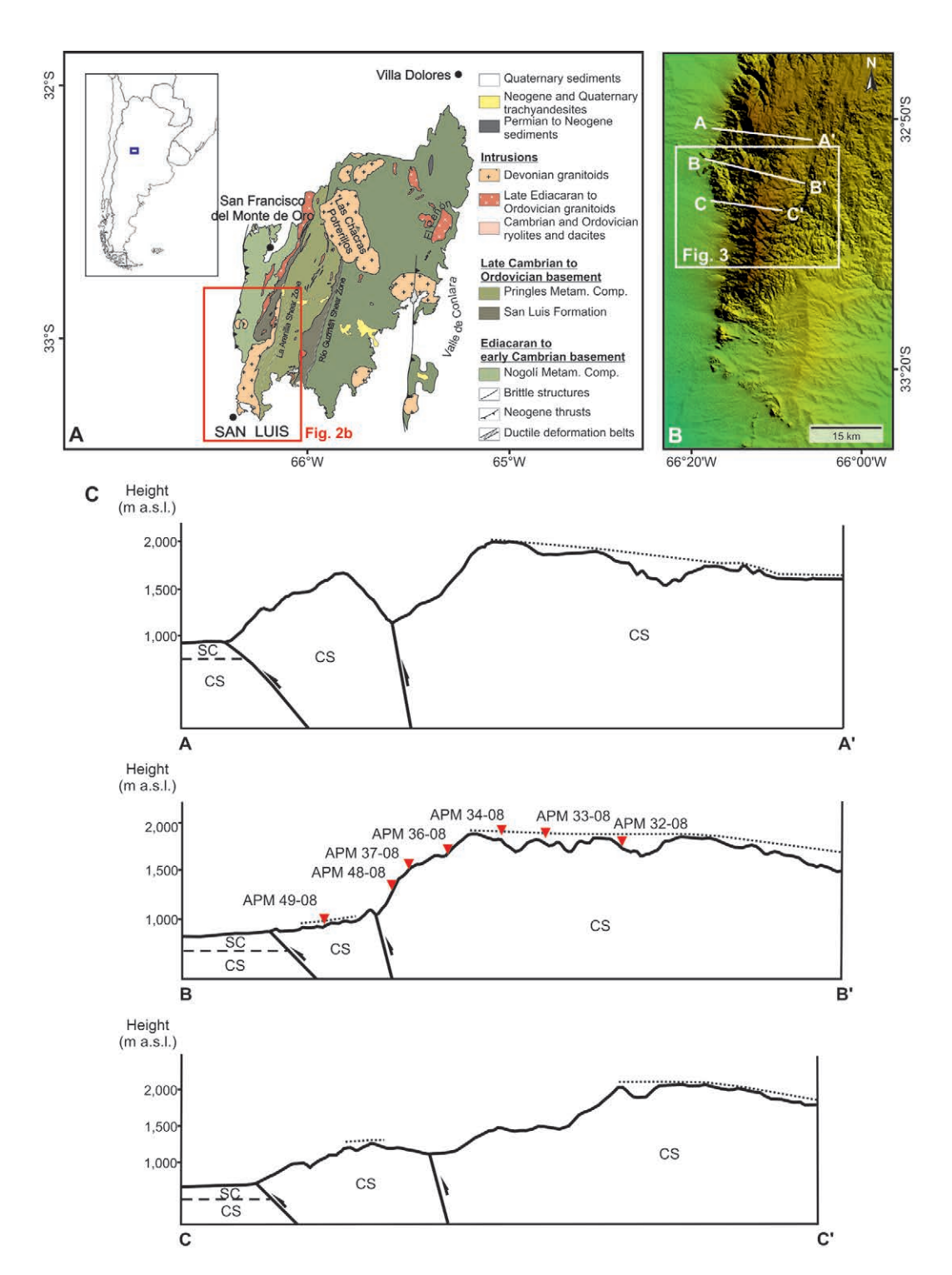


FIG. 2. A. Geological sketch map of the Sierra de San Luis (study area marked by red rectangle); B. SRTM elevation model of southern Sierra de San Luis with cross-section lines in figure 2c and location of regional map depicted in figure 3; C. Cross-section of studied transect, sample location and location of inferred major fault zones (location of fault zones based on geological maps from San Luis and San Francisco del Monte de Oro (Costa *et al.*, 2000, 2001a); note that major fault zones illustrated here does not have a clear, single surface expression). CS: crystalline basement; SC: sedimentary cover; dotted lines: paleosurfaces.

Basement blocks consist of late Precambrian to early Paleozoic metamorphic and igneous rocks showing a topographic asymmetry represented by a steep western and a gentle eastern slope (Fig. 2), being the latter usually characterized by erosional paleosurfaces remnants. This topographic asymmetry is interpreted to be linked to Neogene uplift along reverse faults with listric geometry (González Bonorino, 1950; Jordan and Allmendinger, 1986; among others), which are usually located at the steeper western sides of the ranges (Fig. 1). The Neogene uplift resulted from the incorporation of the Juan Férnandez Ridge into the subduction of the Nazca plate, causing southeastwardpropagating flat-slab subduction beneath the Pampean region (Yáñez et al., 2001) and low heat flow into the crust of the overriding plate as well (Dávila and Carter, 2013; Collo et al., 2015).

Thermochronological data which allow a quantitative evaluation of cooling and exhumation of the basement blocks are still scarce in the southeastern Sierras Pampeanas (Jordan *et al.*, 1989; Coughlin *et al.*, 1998; Löbens *et al.*, 2011, 2013a, b; Bense *et al.*, 2013, Dávila and Carter, 2013; Richardson *et al.*, 2013; Enkelmann *et al.*, 2014; Collo *et al.*, 2015). Hence, the evolution of these ranges since the late Paleozoic is still a matter of ongoing debate (*e.g.*, Jordan *et al.*, 1989; Carignano, 1999; Löbens *et al.*, 2011; Dávila and Carter, 2013; Enkelmann *et al.*, 2014; Rabassa *et al.*, 2014).

This investigation provides thermochronological data of the western part of the Sierra de San Luis, which are complemented with K-Ar illite fine-fraction dating on fault gouges. Based on this, our work aims to constrain the cooling and exhumation history of this part of the range since the Late Paleozoic. In addition, this work aims to check the possible morphotectonic evolution scenarios, especially in the context of the onset of brittle deformation and the formation of paleolandsurfaces.

#### 2. Geological and Morphotectonic Setting

Geological studies of the Sierra de San Luis have traditionally been focused on the tectonometamorphic evolution of the crystalline basement, which is considered to be completed by Early Carboniferous times (Criado Roque *et al.*, 1981; Ortiz Suárez *et al.*, 1992; Von Gosen, 1998; Steenken *et al.*, 2004). Deformation of the basement was dominated by

brittle deformation ever since, leading to characteristic N-S trending fault blocks bounded by major reverse faults during Cenozoic crustal shortening (Fig. 1).

The basement of the Sierra de San Luis consists mainly of metamorphic and igneous rocks, including schists, migmatites, gneisses and phyllites (e.g., Ortiz Suárez et al., 1992; Von Gosen, 1998; Costa et al., 1998a, 20001, 2001a, 2005; Sato et al., 2003; González et al., 2004), which are intruded by granitoids of Cambrian to Early Carboniferous age (Llambías et al., 1991; Ortiz Suárez et al., 1992; Sims et al., 1997; Costa et al., 1998a; Von Gosen et al., 2002; Siegesmund et al., 2004; Morosini et al., 2017, among others). This basement was formed by accretion of multiple terranes during several orogenic cycles (i.e., Pampean, Famatinian and Achalian Orogeny) between the late Proterozoic and early Paleozoic (e.g., Ramos, 1988; Sims et al., 1998; Ramos et al., 2002; Steenken et al., 2004, 2010; Miller and Söllner, 2005; Ramos, 2008).

In the late Paleozoic, the San Luis range was part of the continental Paganzo basin, whose stratigraphic record is widespread along the Sierras Pampeanas (Salfity and Gorustovic, 1983; Mpodozis and Ramos, 1989; Ramos *et al.*, 2002; Limarino and Spalletti, 2006; Ramos, 2009). In the study region, the record of Paganzo strata is scarce, although minor outcrops are present in the Bajo de Véliz depression in the northeastern Sierra de San Luis (Hünicken *et al.*, 1981) (Fig. 2a).

Subsequent Mesozoic rifting along reactivated Paleozoic structures led to the development of continental basins and deposition of Mesozoic clastic sediments to the west and around the Sierra de San Luis (Criado Roque, 1972; Schmidt *et al.*, 1995; Costa *et al.*, 2000). Rifting was accompanied by alkaline intraplate volcanism, which is recorded around the Sierra de San Luis (Llambías and Brogioni, 1981). Additionally, López and Solá (1981) described isolated outcrops of rift-related volcanic rocks in the Sierra de San Luis with K-Ar ages of *ca.* 83±5.85 Ma.

Main Andean Cenozoic crustal shortening and flat-slab subduction of the Nazca Plate is inferred to be related to plate reorganization and collision of the Juan Fernández Ridge during the Miocene (Jordan *et al.*, 1983; Yáñez *et al.*, 2001; Ramos *et al.*, 2002), giving rise to uplift of Pampean basement blocks including the Sierra de San Luis. These uplifts were usually controlled by former main bounding faults of the Mesozoic rift system and other relevant

<sup>&</sup>lt;sup>1</sup> Costa, C.H.; Machette, M.N.; Dart, R.; Bastías, H.; Paredes, J.; Perucca, L.; Tello, G.; Haller, K. 2000. Map and database of Quaternary faults and folds in Argentina. *In* International Lithosphere Program, United States Geological Survey (USGS), Open-file report 00-0108: 81 p.

anisotropies of the basement, which were tectonically inverted as a broken foreland (Jordan *et al.*, 1983; Jordan and Allmendinger, 1986; Schmidt *et al.*, 1995; Costa, 1992; Ramos *et al.*, 2002;).

Erosional surface remnants were envisaged as key markers to constrain the geometry and characteristics of the post-Paleozoic structural relief and the associated uplift and exhumation path, as no pre-Quaternary sedimentary cover was developed or preserved atop the ranges (Costa, 1992; Costa et al., 1999). These paleolandsurfaces have been regarded in two ways. González Díaz (1981) and Criado Roque et al. (1981) considered them as a formerly continuous and essentially synchronous surface, which was uplifted and disrupted into several minor surfaces and juxtaposed by faults during the Andean Orogeny. Alternatively, Carignano (1999) and Rabassa et al. (2010, 2014) suggested that erosional paleosurfaces represent diachronous planation episodes, which are confined to different topographic levels and separated by topographic scarps. Based on field observations, the latter authors propose that paleosurface ages should range between Late Paleozoic and Paleogene. Based on few thermochronological data, a similar proposal on diachronous regional paleosurfaces had been previously raised by Jordan et al. (1989).

Neogene faulting activity documented along the western steep scarp of the Sierra de San Luis suggests that this hillslope constitutes the neotectonic uplift of the range, where at least 1000 m of structural relief was built-up since planation surfaces were formed (Costa, 1992; Costa *et al.*, 2001b). On the other hand, recent thermochronological studies in other regions of the Sierras Pampeanas near the Sierra de San Luis indicate that exhumation and cooling associated with uplift since the Cenozoic was considerably small (Löbens *et al.*, 2011; Bense *et al.*, 2013; Enkelmann *et al.*, 2014).

#### 3. Methodology

### 3.1. Thermochronology

"Exhumation" and "uplift" are widespread terms used in the literature to refer to the vertical transport of rock masses. Nevertheless, misinterpretations may arise as it is frequently not clear what these terms refer to. England and Molnar (1990) defined exhumation as the displacement of rocks with respect to the surface. If a crustal thermal profile is assumed, exhumation

rates can thus be derived from thermochronological data (England and Molnar, 1990; Stüwe and Barr, 1998; Ring *et al.*, 1999). Uplift, in turn, is related to vertical movements with respect to the geoid, although the mean sea level can be considered as the reference level as well (England and Molnar, 1990). England and Molnar (1990) further differentiated between "surface uplift" and "uplift of rocks", depending on whether displacements of the surface or displacements of rocks are considered. In this work, exhumation and uplift are considered following these definitions, being the latter related to surface uplift *sensu* England and Molnar (1990).

(U-Th)/He ages from apatite (AHe) and zircon (ZHe) as well as apatite fission track ages (AFT) can be interpreted in terms of an exhumation-induced cooling through low temperature conditions and provide an important tool for quantifying the cooling of rocks as they pass through relatively shallow crustal levels. According to Donelick et al. (1999) and Ketcham et al. (1999), among others, the thermal sensitivity of the apatite fission track method, namely the partialannealing zone (PAZ; Gleadow and Fitzgerald, 1987), ranges between 130 °C and 60 °C. For the (U-Th)/He system of apatite and zircon, this temperature interval is referred to as the partial-retention zone (PRZ) and ranges between 65 °C and 30 °C and 185 °C and 135 °C, respectively (e.g., Baldwin and Lister, 1998; Wolf et al., 1998; Reiners and Brandon, 2006).

The analytical procedure on (U-Th)/He and apatite fission track dating is described in the Appendix. Based on dating results, a two-stage approach of forward and inverse modelling of thermochronological data using HeFTy software (Ketcham, 2005) was followed to model numerically possible t-T paths for individual samples. Especially the combination of fission track data (age and track length distribution) with (U-Th)/He data can provide a diagenetic and sensitive tool for evaluating low-temperature thermal history.

Two boundary conditions were set to the thermal modeling: **1.** the beginning of the time-temperature path was constrained by the zircon (U-Th)/He data and **2.** the end of the time-temperature paths was set to 17 °C, according to annual mean temperatures in the study area (Müller, 1996).

#### 3.2. Fault gouge dating and interpretation

Under brittle conditions, tectonic slip causes the crushing of rocks and grain-size reduction along

faults. In these localized fault zones, the increased area/volume ratio of rock fragments together with fluid circulation favors high chemical reactivity, allowing retrograde processes to produce fault gouges composed of authigenic hydrosilicates such as illite. Thus, the formation time of the authigenic illite in a fault gouge, can be correlated with periods of motion along the fault and thus constrains the timing of faulting where favorable conditions for illite formation are present (*e.g.*, Lyons and Snellenberg, 1971; Kralik *et al.*, 1987; Wemmer, 1991; Solum *et al.*, 2005; Haines *et al.*, 2008; Zwingmann *et al.*, 2010; Surace *et al.*, 2011; Wolff *et al.*, 2012; Bense *et al.*, 2014).

Bense *et al.* (2014) suggested a concept to evaluate the timing of brittle deformation based on K-Ar illite fine-fraction ages from fault gouges, which are developed in non-sedimentary host rocks during retrograde cooling. Following this idea, the interpretation of K-Ar illite ages is constrained by evaluation of several independent parameters, *e.g.*, illite crystallinity, illite polytype quantification, illite grain-size, clay mineralogical observations, K-Ar

muscovite and biotite host-rock cooling ages, as well as low-temperature thermochronological data derived from, *e.g.*, fission track or the (U-Th)/He dating. This allows a better error evaluation of individual methods by highlighting concordant data in multi-methodological datasets, as well as an easier combination of all observations into a consistent regional evolution model. For a detailed discussion of methodological, interpretation and analytical issues, the reader is referred to Bense *et al.* (2014). Further details on data interpretation and analytical procedures are given in the Appendix.

Samples of brittle fault zones across the investigated profile were analysed and dated (Figs. 3, 4, 5, 6; Tables 1, 2, 3), to be linked to fault motions.

#### 4. Results

## 4.1. Thermochronology

Eight samples, mainly from granitic rocks of the crystalline basement were collected along a

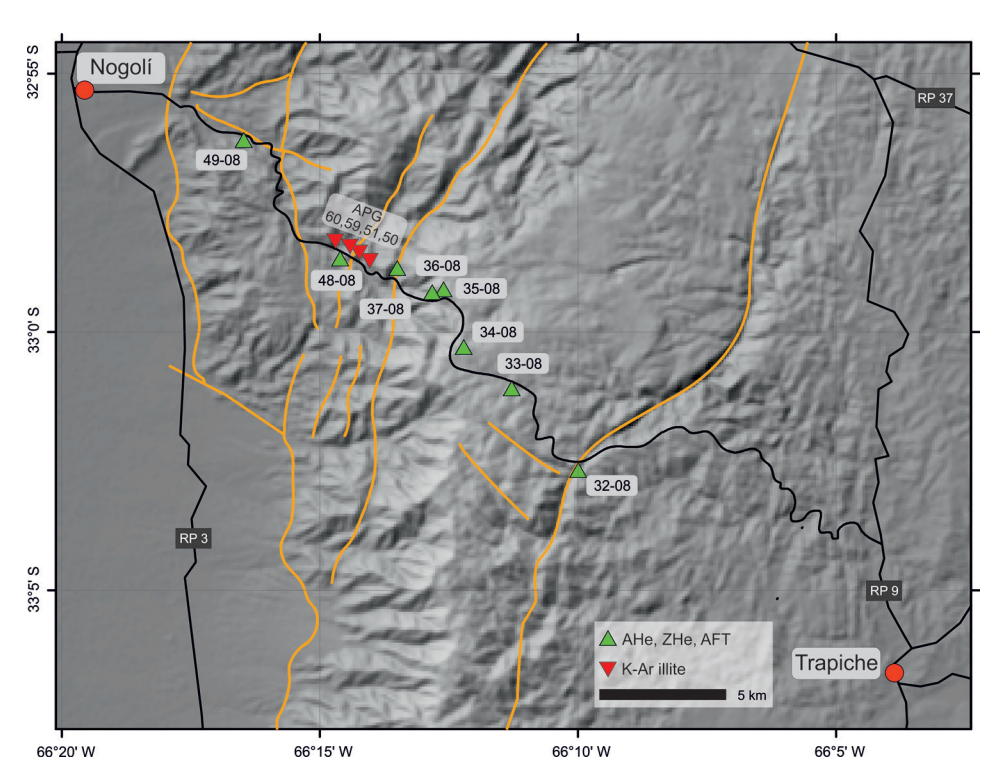


FIG. 3. Simplified DEM-based map of the study area with locations of thermochronological samples (green triangles) and K-Ar illite fault-gouge samples (red triangles). For location of map extent see figure 2.

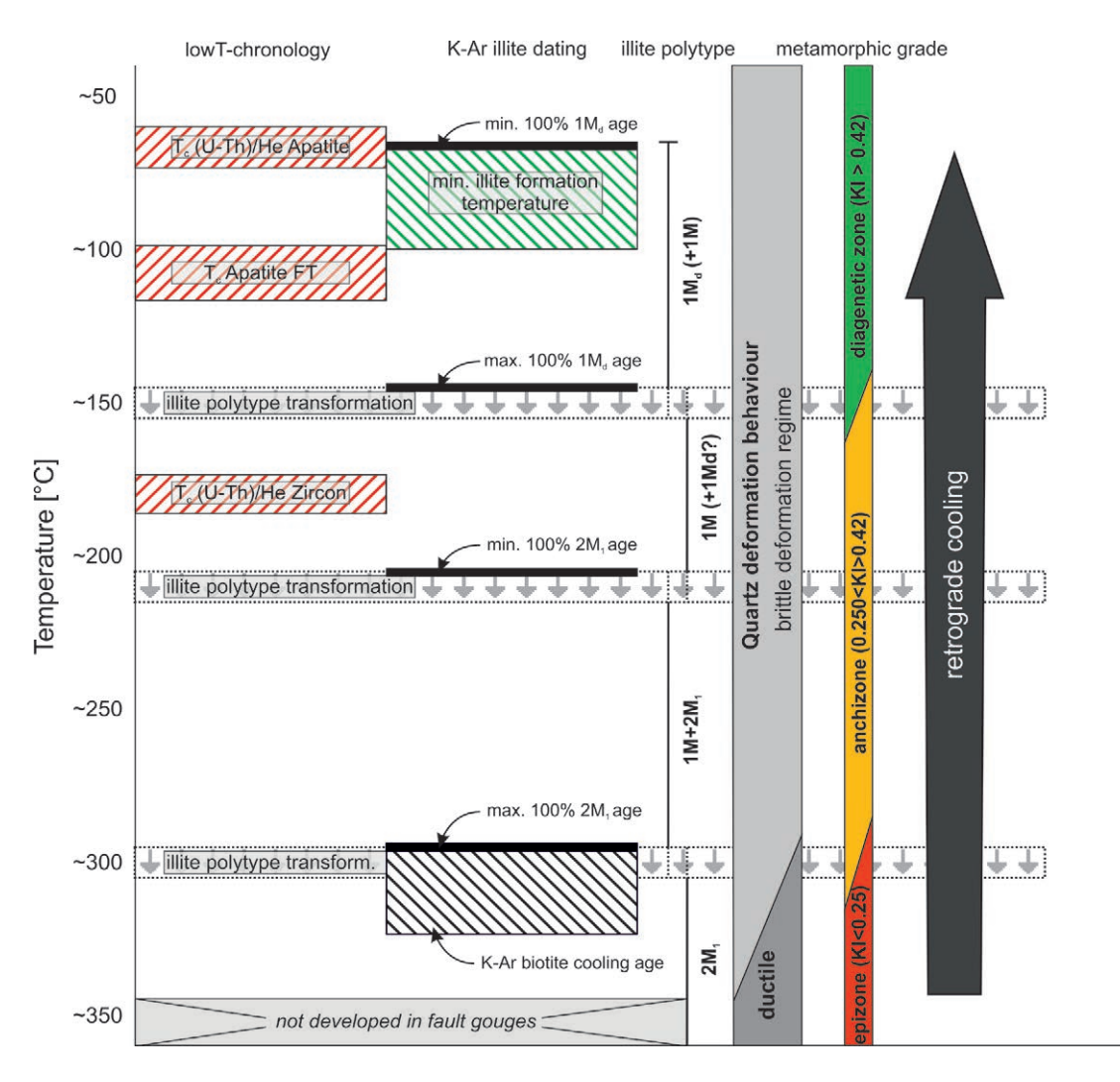


FIG. 4. Scheme for the interpretation of K-Ar illite fine fraction ages and polytype quantification data in combination with regional cooling data derived from (U-Th)/He, apatite fission track and K-Ar biotite method. The illite polytype transition zone marks the irreversible transition from one respective polytype to another under prograde conditions. Thus, under retrograde conditions there will always be a mixture of polytypes in the respective metamorphic zone. The temperatures for the transition between polytype-deformation-and metamorphic regimes have to be considered as continuously with not exact constrained temperature boundaries. The ages for the fault gouge fine-fraction (2-6 μm; 2 μm and <0.2 μm) are not indicated in this figure but would lie between the maximum 100% 2M₁ age and the minimum 100% 1M₂ age (note that this scheme involve simplifications. Additionally scheme is mainly concerted on interpretation of retrograde illite from fault gouges in non-sedimentary rocks; IC=illite crystallinity; T₂=effective closure temperature; temperatures for respective system see Reiners and Brandon (2006), approximated illite polytype transformation temperatures according to Hunziker *et al.* (1986), Yoder and Eugster (1955), Velde (1965), Weaver (1989); temperature ranges of brittle and ductile deformation behavior of quartz taken from Passchier and Trouw (2005), IC=values for diagenetic zone, anchi-and epizone according to Kübler (1967); closure temperature of K-Ar biotite system according to Purdy and Jäger (1976)).

transect encompassing the western slope and upper parts at the South of the Sierra de San Luis (Figs. 2, 3, Tables 4 and 5). Mean zircon (U-Th)/He ages range from the Late Carboniferous to Middle Triassic (313 to 229 Ma). Ages show no clear correlation with elevation (Fig. 7, Table 5) and, due to the high scatter of individual ages, single ZHe ages are not interpreted to represent distinct events. Instead, ZHe ages are used as constraints for the modelling of the thermal history of individual samples (see below).

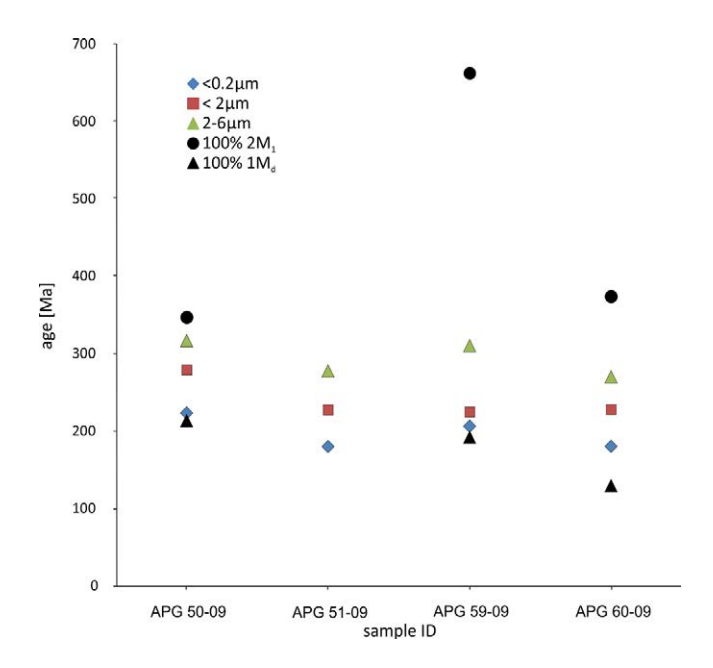


FIG. 5. K-Ar ages of all analyzed grain-size fractions and samples as well as extrapolated ages for the 2M<sub>1</sub> and 1M<sub>d</sub> polytypes. All samples were taken from well-developed clay-gouges from small-scale faults in the middle part of the western hillslope (Fig. 3). Note the increase in illite age with increase in grain-size. The 100% 2M<sub>1</sub> and 100% 1M<sub>d</sub> ages are interpreted to represent the begin of deformation along the fault, respectively to represent the end of deformation and/or cooling below illite formation temperatures (more details are discussed in the text).

Apatite fission track ages range from Early Triassic to Early Jurassic (251 to 192 Ma; Table 4 and Fig. 8). Again, no correlation between age and elevation as expected for undisturbed elevation profiles (Fitzgerald *et al.*, 2006) is recognizable. The youngest apparent ages (196 Ma and 192 Ma) can be found in the middle part of both slopes (Table 4).

Investigated samples are characterized by distinct shortened tracks with an unimodal track length distribution and a mean track lengths between 11.9  $\mu m$  and 12.9  $\mu m$  with a standard deviation of 0.9-1.5  $\mu m$  (Table 4 and Fig. 8). The mean etch-pit diameters (Dpar values) of the seven samples are between 1.79  $\mu m$  and 2.09  $\mu m$  (Table 4).

Mean apatite (U-Th)/He ages along the San Luis transect range between the Middle Triassic and the Middle Cretaceous (286 to 105 Ma; Table 5 and Fig. 7). There is no correlation between age and elevation on either the western slope or on the eastern flank (Fig. 2). The youngest age (105 Ma) was found at the base of the western slope. Generally, apatite (U-Th)/He ages are younger or overlap within their 1σ-error with their corresponding AFT age. An exception is given by APM 48-08 and 32-08, as

AHe ages are older than corresponding AFT ages, contradicting the normal age trend of AFT>AHe (Table 5 and Fig. 7).

## 4.2. K-Ar dating

Four small-scale fault zones along the Nogoli-Río Grande transect (Fig. 3) were sampled and dated by the K-Ar illite method in several grainsize fractions. Additionally, illite polytype quantification, illite crystallinity determination and mineralogical classification of gouges were done by X-ray diffraction.

In total, twelve K-Ar ages for the grain-size fractions of  $<0.2 \,\mu\text{m}$ ,  $<2 \,\mu\text{m}$  and 2-6  $\mu\text{m}$  from four samples were analysed. Samples were taken from associated small-scale faults in the middle part of the western hillslope (Fig. 3), where the best-exposed fault gouges were observed. No reliable kinematic information of fault slip data sets could have been surveyed, just slickenlines geometry.

Samples were exclusively taken from clay fault gouges developed in macroscopically muscovite free crystalline host rocks. Sampled locations

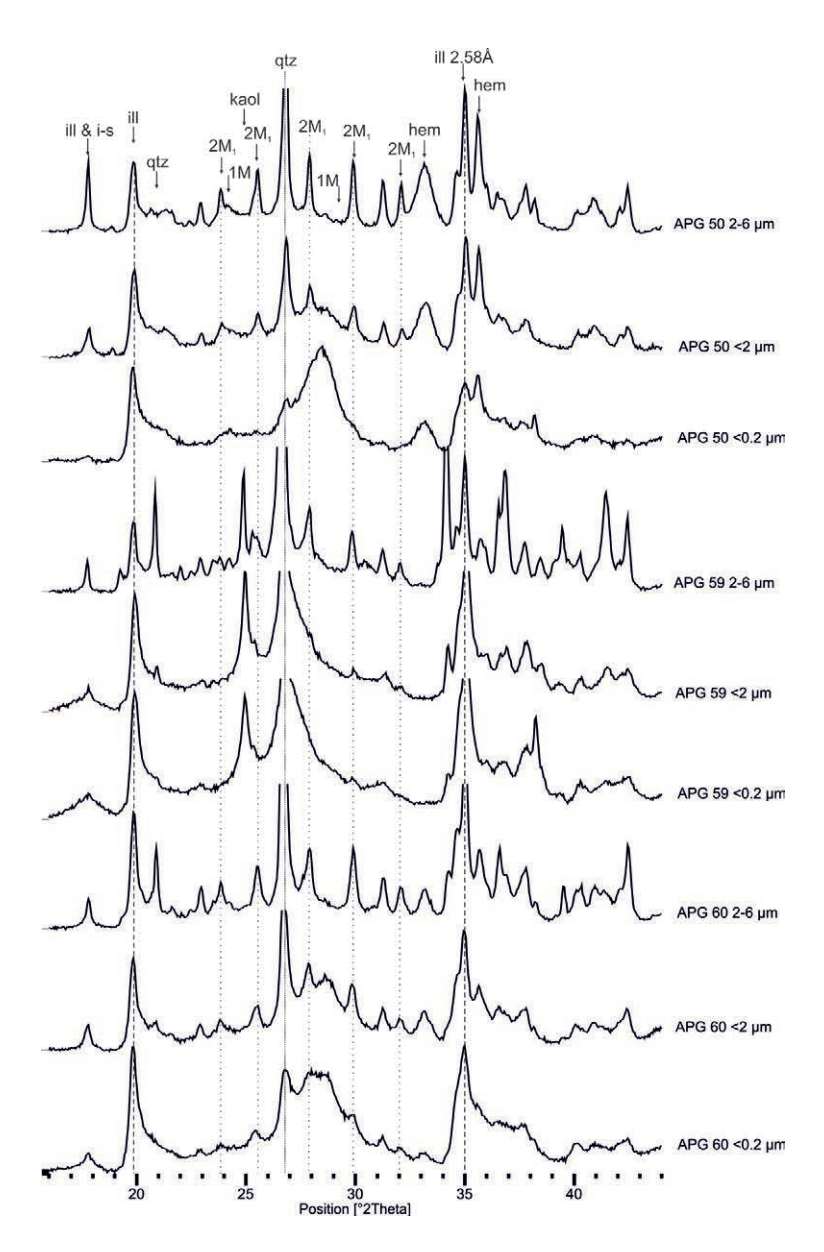


FIG. 6. XRD pattern derived from randomly oriented samples with indicated positions of 2M<sub>1</sub> and 1M polytype specific peaks. Other phases are indicated as follows: illite (ill), Illite-Smectite (i-s), quartz (qtz), kaolinite (kaol) and hematite (hem).

yield well developed clay gouges, in some cases with small grains of residual rock material. The monomineralic grains are only a few millimetres in diameter and consist almost exclusively of quartz. Polymineralic rock fragments were not observed within sampled material. Gouge thicknesses range from several millimetres up to several centimetres, but mostly vary between 0.5-2 cm. Sampled gouges have monochrome brownish to reddish colours.

K-Ar ages range from Early Pennsylvanian to Early Jurassic times (315-178 Ma). The age-analysis plot of all analysed samples is depicted in figure 5 and data are listed in table 1. All samples show a time interval span between fractions ranging from 18.7 Ma up to 84.7 Ma (Fig. 5). No overlapping ages could be observed within one sample. Radiogenic  $^{40}\mathrm{Ar}$  content ranges from 80.3% to 97.7%, potassium ( $\mathrm{K}_2\mathrm{O}$ ) content ranges from 1.26% to 6.17% (Table 1),

TABLE 1. K-Ar AGES, ILLITE CRYSTALLINITY AND ILLITE POLYTYPISM OF THE INV	ESTIGATED MINERAL
FRACTIONS	

Sample	Grain		K	-Ar Data	ı		Illite c	rystallinity	Illite polytypism		
	fraction	K <sub>2</sub> O [wt%]	<sup>40</sup> Ar* [nl/g] STP	<sup>40</sup> Ar*	Age [Ma]	±2σ-error [Ma]	air dry [Δ°2θ]	glycolated [Δ°2θ]	2M <sub>1</sub> , 1M, 1M <sub>d</sub>		
	<0.2 μm	1.26	9.60	82.58	222.0	6.0	0.226	0.316	9%, 7%, 84%		
50-09	<2 μm	2.48	24.04	92.18	278.0	3.0 9.5 0.22		0.206	45%, 5%, 49%		
	2-6 μm	4.21	46.80	92.61	315.4	7.0	0.162	0.158	79%, 5%, 15%		
	<0.2 μm	1.77	10.74	80.34	178.9	4.9	0.565	0.748			
51-09	<2 μm	2.70	21.02	91.47	226.5	5.0	0.425	0.496	no polytype analysis performed		
	2-6 μm	3.12	30.07	97.16	276.5	6.1	0.312	0.338	performed		
	<0.2 μm	4.56	31.96	94.05	205.2	4.9	0.579	0.651	3%, 4%, 93%		
59-09	<2 μm	4.76	36.60	94.43	223.9	5.1	0.427	0.655	7%, 5%, 88%		
	2-6 μm	6.17	66.98	97.27	308.7	6.5	0.256	0.173	25%, 5%, 70%		
	<0.2 μm	2.77	16.81	86.00	179.0	4.2	0.294	0.275	20%, 4%, 76%		
60-09	<2 μm	3.80	29.63	93.11	226.9	7.0	0.276	0.292	46%, 4%, 49%		
	2-6 μm	5.30	49.55	97.70	268.8	5.5	0.195	0.218	53%, 4%, 43%		

TABLE 2. RESULTS OF X-RAY DIFFRACTION ANALYSES FROM THE SAMPLE MATERIAL FRACTIONS.

Sample No.	Grain Size Fraction	Illite	Chlorite	Kaolinite	Smectite	Quartz	Feldspar	Others <sup>1</sup>
	<0.2 μm	+	-	-	++	-	-	Halloysite o/-
50-09	<2 μm	+	-	-	++	-	-	Halloysite o/-
	2-6 μm	o	-	-	+	-	-	Halloysite o/-
	<0.2 μm	+	-	+	+	-	-	-
51-09	<2 μm	+	-	+	0	+	-	-
	2-6 μm	+	-	+	-	++	0/-	-
	<0.2 μm	++	-	++	0/-	-		-
59-09	<2 μm	++	-	++	0/-	0/-	-	-
	2-6 μm	++	-	++	-	0/-	0/-	-
	<0.2 μm	++	-	-	++	-	-	Halloysite o/-
60-09	<2 μm	++	-	-	+	-	-	Halloysite o/-
	2-6 μm	+	-	-	0/-	+	0/-	Halloysite o/-

++: dominant; +: abundant; o: less abundant; o/-: unclear, possibly traces; -: none; 1: identified by TEM.

indicating reliable analytical conditions for all analyses samples. XRD analyses of all samples confirm that illite, smectite and kaolinite are the major clay mineral components in the various fractions (Table 3 and Fig. 6). The presence of quartz is restricted to the fractions  $<2~\mu m$  and  $2-6~\mu m$ ,

and none is found in the  $<\!0.2~\mu m$  fraction. Restricted to the 2-6  $\mu m$  fractions some samples show minor traces of potassium feldspar. These observations were confirmed by TEM analysis. Additionally, TEM analyses also reveal traces of halloysite (Table 2).

TABLE 3. CALCULATED 2M, END-MEMBER AGES.

6 1	Extrapolated Age (Ma)							
Sample	100% 2M <sub>1</sub>	0% 2M <sub>1</sub>						
APG 50-09	346	212						
APG 59-09	661	191						
APG 60-09	372	128						

Extrapolated ages for hypothetical samples consisting of 100% and 0% 2M, illite respectively.

Glycolated XRD analyses were carried out to investigate the potential occurrence of expandable mixed-layers of illite and smectite. Major amounts of illite/smectite were found in all fractions of sample APG 50-09. Except for sample APG 50-09, illite/smectite mixed-layers are nearly absent in the 2-6  $\mu$ m fractions (Table 1). Considerable amounts of smectite could only be found in the <0.2  $\mu$ m fraction.

## 4.3. Illite crystallinity (IC)

The IC, expressed as Kübler Index (KI), of all analysed samples varies from 0.155  $\Delta^{\circ}2\theta$  to 0.530  $\Delta^{\circ}2\theta$  (Table1). KI values from the air-dried <0.2  $\mu m$  fractions indicate that two samples developed under diagenetic conditions. In contrast, the fractions of <2  $\mu m$  and 2-6  $\mu m$  yielded anchi- to epimetamorphic values. Variations in the  $\Delta^{\circ}2\theta$  between the glycolated and the air-dried measurements correspond to the presence of illite/smectite mixed-layers (Table 1). No systematic variation with respect to the sample location was observed. The absence of very low IC together with fact that gouges were taken from macroscopically muscovite free host-rock indicate that grain-size fractions are not contaminated by muscovite phases.

## 4.4. Illite polytypism

All samples used for the illite polytype quantification show a random orientation expressed by a low

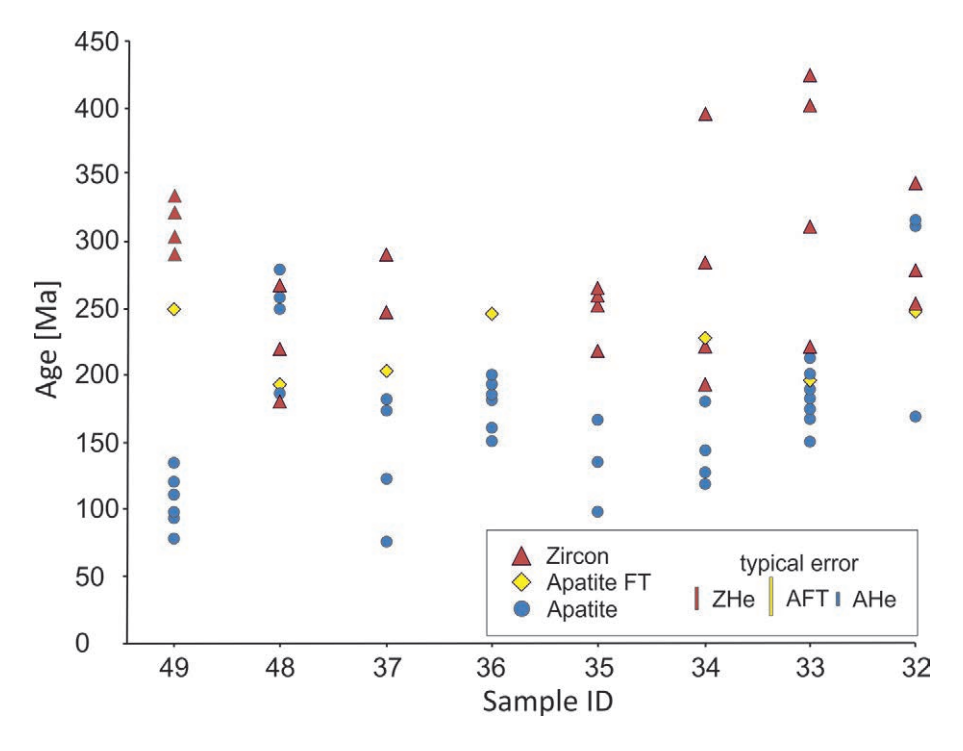


FIG. 7. Compilation of zircon and apatite (U-Th)/He single-grain ages and AFT ages. Generally ages scatter, but correlate with the respective temperature range of the used system (ZHe>AFT>AHe ages). A correlation between age and elevation, as expected for undisturbed elevation profiles (Fitzgerald *et al.*, 2006), can only be observed for some neighboring samples (*e.g.*, between samples 35, 34 and 33). This is interpreted to be the result of segmentation of the transect into several, individual fault blocks (see also figure 2).

TABLE 4. FISSION TRACK DATA.

Sample No. (rocktype)	Latitude Longitude	Elevation (m) a.s.l.	n	$\rho_{s}$	$N_s$	$\rho_{_{\rm I}}$	$N_{_{\rm I}}$	$\rho_{\text{d}}$	$N_d$	P(X <sup>2</sup> ) (%)	Age (Ma)	±1σ (Ma)	MTL (μm)		N	Dρar (μm)
APM 32-08 (granite)	066°09.999° 33°02.669°	1.811	25	15.9	1.025	7.9	514	7.80	7.368	42.1	246.9	23.1	12.3	1.4	50	1.79
APM 33-08 (granite)	066°11.293° 33°01.090°	1.947	23	33.6	2.051	21.4	1.307	7.83	7.368	58.7	195.6	17.0	12.3	0.9	50	1.85
APM 34-08 (granite)	066°12.223° 33°00.285°	2.085	23	16.4	1.167	8.6	616	7.54	7.368	26.4	227.0	21.5	12.4	1.5	48	1.93
APM 36-08 (migmatite)		1.702	25	22.4	1.907	11.1	950	7.63	7.368	11.7	245.3	22.6	12.5	1.0	50	2.05
APM 37-08 (mica schist)	066°13.505° 32°58.760°	1.503	25	34.3	2.734	20.7	1.647	7.69	7.368	64.5	203.0	17.3	12.3	0.9	50	2.09
APM 48-08 (granite)	066°14.608° 32°58.581°	1.269	24	32.1	3.102	20.4	1.972	7.67	7.368	42.0	192.1	16.2	11.9	1.3	50	1.91
APM 49-08 (granite)	066°16.479° 32°56.282°	981	22	19.8	1.745	9.8	863	7.87	7.368	28.3	251.3	22.9	12.9	1.2	50	1.84

Presented ages are central ages  $\pm 1\sigma$  (Galbraith and Laslett, 1993); ages were calculated using zeta calibration method (Hurford and Green, 1983); glass dosimeter CN-5, and zeta value of S.L. is 323.16 $\pm 10.1$  A cm- $^2$ ; zeta error was calculated using ZETAMEAN software (Brandon, 1996); **n**: number of dated apatite crystals;  $\rho_s/\rho_i$ : spontaneous/induced track densities (×105 tracks cm $^2$ );  $\rho_a$ : number of tracks counted on dosimeter;  $N_s/N_i$ : number of counted spontaneous/induced tracks;  $N_a$ : number of tracks counted on dosimeter; **P(X** $^2$ ): probability obtaining chi-squared value (X $^2$ ) for n degree of freedom (where n is the number of crystals -1); **MTL**: mean track length; **SD**: standard deviation of track length distribution; **N**: number of tracks measured; **Dpar**: etch pit diameter.

(002)/(020) illite ratio as well as low (004) illite intensity. XRD tracings of random powders from all samples presented in this study contain a mixture of illite polytypes  $2M_1$ , 1M and  $1M_d$ . The analysed illite fractions are composed mainly of  $1M_d$  and  $2M_1$  polytypes. The  $1M_d$  polytype is dominant in the <0.2  $\mu$ m fractions throughout all analysed samples. In the <2  $\mu$ m fraction, the  $1M_d$  and  $2M_1$  polytypes are observed as the dominant phases. The 2-6  $\mu$ m fractions are mostly made up of  $2M_1$  illite. The 1M illite content is subordinate (maximum of 7%) and more or less constant for all analyzed grain-size fractions and samples (Table 1).

In TEM (transmission electron microscopy) and SAED (selected area electron diffraction) analyses on sample APM 59-09, it was not possible to identify 1M illite, which may be attributed to the small TEM sample volume. However, other authors also reported difficulties to find the 1M polytype proposed by XRD studies during TEM analysis (*e.g.*, Peacor *et al.*, 2002; Solumn *et al.*, 2005).

The relationship of increasing K-Ar ages with increasing grain size (see above and Table 1 and Fig. 5)

is consistent with an increasing content of the  $2M_1$  illite polytype, which was formed in the earlier fault history under higher temperatures. The increase in  $2M_1$  is accompanied by a decrease in  $1M_d$  illite, as it was formed during the late fault history under lower temperatures. Additionally, polytype content correlate with obtained KI values, showing smaller KI-values (higher crystallinity) for samples with higher  $2M_1$  content (Table 2).

Based on the calculated polytype compositions of the samples, we extrapolated the "end-member" age of the  $1 \rm{M_d}$  polytype and the  $2 \rm{M_1}$  polytype (hypothetically samples which consist of 0%  $2 \rm{M_1}$  illite and 100%  $2 \rm{M_1}$  illite, respectively) by plotting the age of each individual grain-size fraction of a fault gouge sample against the  $2 \rm{M_1}$  illite content (Fig. 9 and Table 1). These plots show a coefficient of determination (R²) always larger than 0.9, confirming a clear linear relationship between age and  $2 \rm{M_1}$  polytype content.

Potential errors in polytype quantification may have been caused by smectite. XRD reflections from smectite exhibit overlap with illite polytype specific

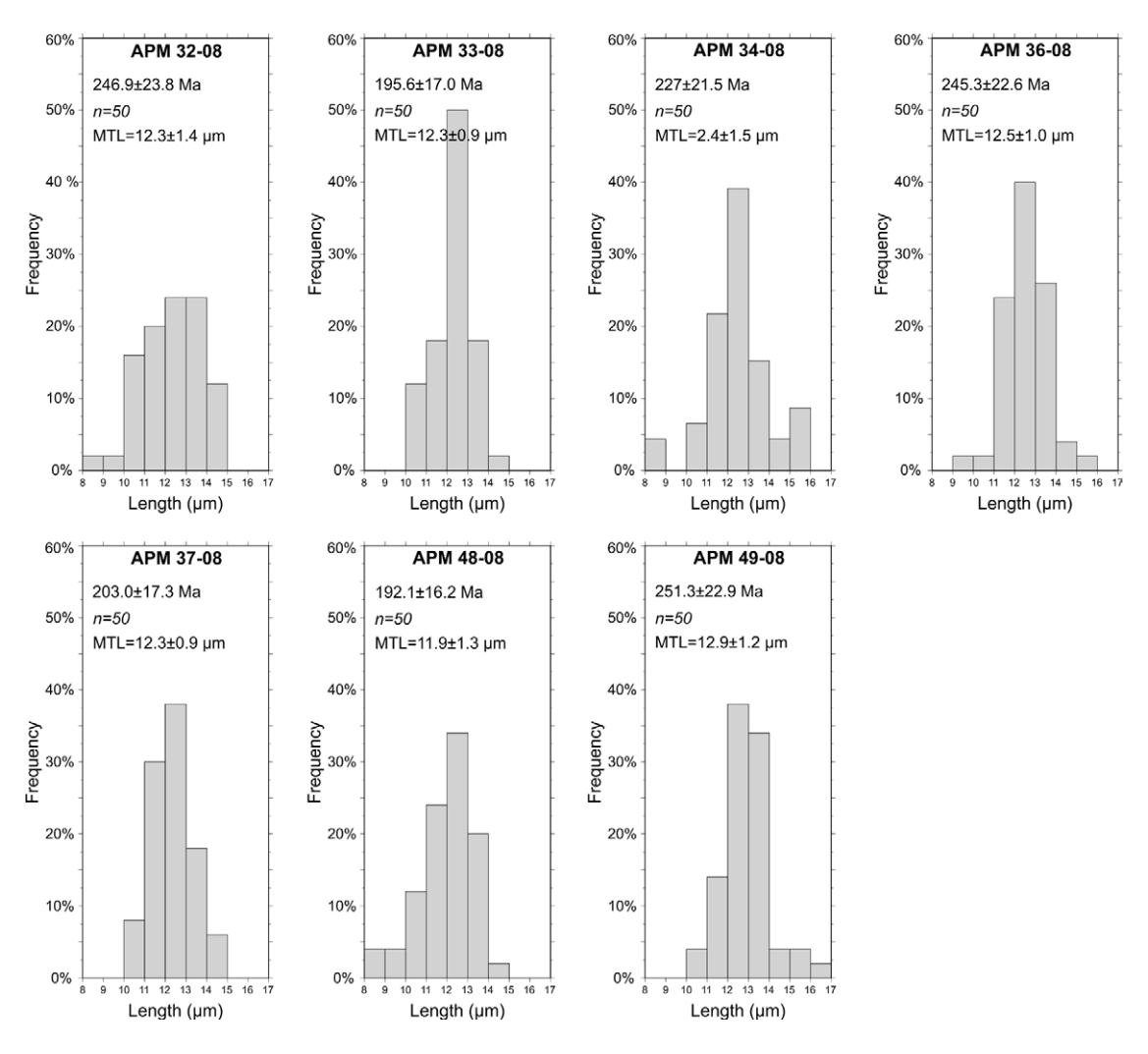


FIG. 8. Track length distribution of the investigated samples. The amount of measured confined tracks is given by n. The apparent age of each sample is shown in italic letters. Elevation and FT parameters of samples are shown in table 4.

reflections (Fig. 6; Grathoff and Moore, 1996). In the case of superposition of smectite reflections on illite peaks, the illite content might be overestimated. As a consequence, polytype quantification as well as extrapolated 100% 2M<sub>1</sub> and 0% 2M<sub>1</sub> illite ages are subjected to error, possibly greater than the conservatively assumed general methodological error for polytype quantification of 2-5% (Grathoff and Moore, 1996). However, polytype quantification is in good accordance with other parameters, such as grain-size age, illite crystallinity and K-Ar age, indicating the consistency of the data set. Even most of the extrapolated polytype end-member ages (Table 3) are in good accordance with K-Ar mica

cooling ages (see discussion). Non-deformational illite formation by fluid percolation cannot be excluded but is unlikely due to the consistency of the data set.

## 5. Discussion

## 5.1. Thermal modelling

Based on the individual cooling paths derived from HeFTy modelling, a regional thermal history for the entire transect was compiled and is shown in figure 10. Cooling below the PRZ<sub>z</sub> temperatures ( $\approx$ 175 °C) over the whole transect started in Late

TABLE~5.~ZIRCON~AND~APATITE~(U-Th)/He~DATA~OF~THE~SAMPLES~FROM~THE~NOGOL'I-RIO~GRANDE~PROFILE..

Sample	He [ncc]	s.e. %	<sup>238</sup> U mass [ng]	s.e. %	<sup>232</sup> Th mass [ng]	s.e. %	Th/U	Sm mass [ng]	s.e. %	Corr. Ft USED	Uncorr. [Ma]	Ft- Corr. [Ma]	1s [Ma]	Sample weighted average age [Ma]
Zircon														
APM 32-08	41.203	1.6	1.527	1.8	0.906	2.4	0.59	0.183	5.5	0.694	192.7	277.6	14.2	
(granite)	20.928	1.6	0.582	1.8	0.247	2.4	0.42	0.036	6.1	0.770	264.4	343.3	14.2	
	12.423	1.6	0.547	1.8	0.192	2.4	0.35	0.032	6.1	0.679	171.0	251.8	13.44	291.6
APM 33-08	90.940	1.6	4.444	1.8	0.739	2.4	0.17	0.070	8.1	0.726	160.8	221.7	10.5	
(granite)	11.792	1.6	0.431	1.8	0.241	2.4	0.56	0.023	11.1	0.633	196.8	310.8	18.52	266.2
APM 34-08	9.649	1.6	0.383	1.8	0.235	2.4	0.61	0.021	6.7	0.633	179.3	283.0	16.83	
(granite)	3.268	1.7	0.231	1.9	0.007	2.8	0.03	0.001	19.7	0.602	115.4	191.7	12.37	
	4.462	1.7	0.266	1.8	0.023	2.5	0.09	0.010	7.7	0.607	134.7	222.0	14.15	232.2
APM 35-08	53.820	1.6	2.308	1.8	0.605	2.4	0.26	0.343	5.8	0.818	178.9	218.8	7.84	
(gneiss)	26.703	1.6	1.068	1.8	0.292	2.4	0.27	0.115	6.5	0.753	191.2	253.9	11.1	
	69.049	1.6	2.352	1.8	1.759	2.4	0.75	0.421	5.5	0.772	202.9	262.7	10.72	
	29.805	1.6	1.142	1.8	0.712	2.4	0.62	0.164	6.5	0.696	185.4	266.2	13.53	253.6
APM 37-08	23.232	1.6	0.823	1.8	0.359	2.4	0.44	0.024	32.3	0.718	208.2	289.9	13.94	
(mica schist)	20.578	1.6	0.832	1.8	0.285	2.4	0.34	0.026	31.4	0.757	186.4	246.4	10.64	271.1
APM 48-08	29.467	1.6	1.229	1.8	0.487	2.4	0.4	0.109	5.2	0.713	178.7	250.6	12.22	
(granite)	205.521	1.6	7.045	1.8	1.868	2.4	0.27	0.372	5.5	0.835	222.9	266.9	9.03	
	512.118	1.6	25.276	1.8	5.105	2.4	0.2	1.210	5.2	0.877	158.0	180.2	5.36	
	110.013	1.6	4.842	1.8	1.055	2.4	0.22	0.480	5.1	0.805	176.2	218.9	8.19	
	119.681	1.6	5.978	1.8	1.517	2.4	0.25	0.475	5.4	0.856	154.3	180.2	5.7	228.6
APM 49-08	80.278	1.6	1.890	1.8	2.560	2.4	1.35	0.127	5.1	0.812	261.0	321.5	11.47	
(granite)	203.857	1.6	4.418	1.8	6.572	2.4	1.49	0.289	5.1	0.832	276.7	332.6	11.07	
	110.448	1.6	2.508	1.8	4.243	2.4	1.69	0.195	5.1	0.839	255.4	304.6	9.89	
	122.269	1.6	3.146	1.8	4.156	2.4	1.32	0.162	5.2	0.831	240.6	289.6	9.69	313.1
Apatite				-										
APM 32-08	0.263	2.1	0.003	21.2	0.014	3.7	5.32	0.244	6.1	0.852	265.8	311.9	24.07	
(granite)	0.323	2.1	0.014	4.1	0.021	3.3	1.52	0.195	6.1	0.784	132.3	168.7	8.06	
	1.533	1.7	0.014	4.1	0.127	2.5	8.98	0.250	5.9	0.864	271.7	314.6	10.59	285.6
APM 33-08	4.699	1.7	0.234	1.8	0.012	4	0.05	0.507	5.1	0.843	159.3	188.9	6.33	
(granite)	7.967		0.401	1.8	0.069	2.5	0.17	1.129	5.6	0.838	152.8	182.2	6.14	
	3.778	1.7	0.169	1.9	0.023	3.2	0.13	0.562	5.2	0.805	172.0	213.8	8.06	
	3.162	1.7	0.169	1.8	0.017	2.9	0.1	0.237	5.5	0.884	147.9	167.3	4.96	
	3.554	1.7	0.214	1.8	0.010	4.3	0.05	0.584	4.8	0.876	131.6	150.2	4.56	
	7.168		0.317	1.8	0.022	2.8	0.07	0.670	5.4	0.896	178.6	199.4	5.66	
	11.524	1.6	0.482	1.8	0.044	2.6	0.09	0.648	5.4	0.890	188.5	211.8	6.11	
	3.136		0.165	1.8	0.030	2.7	0.18	0.356	5.4	0.843	146.6	174.0	5.82	188.7

continuation table 5.

Sample	He [ncc]	s.e. %	<sup>238</sup> U mass [ng]	s.e. %	<sup>232</sup> Th mass [ng]	s.e. %	Th/U	Sm mass [ng]	s.e. %	Corr. Ft USED	Uncorr. [Ma]	Ft- Corr. [Ma	1s [Ma]	Sample weighted average age [Ma]
APM 34-08	1.654	1.8	0.080	1.9	0.003	6	0.04	0.326	5.7	0.898	161.5	179.9	5.27	
(granite)	0.230	2.1	0.007	9.7	0.019	3.4	2.7	0.972	4.7	0.831	98.6	118.5	6.06	
	0.109	2.8	0.006	9	0.002	7	0.39	0.019	9.8	0.876	125.8	143.5	12.15	
	0.609	1.9	0.044	2.1	0.005	4.7	0.1	0.096	6.6	0.855	109.2	127.7	4.48	142.4
APM 35-08	0.581	1.8	0.034	2.7	0.008	4.9	0.23	0.018	5.4	0.804	134.0	166.7	7.08	
(gneiss)	0.082	2.6	0.007	8.4	0.011	2.7	1.62	0.020	3	0.753	73.4	97.5	7.13	
	0.030	3.8	0.003	20.5	0.003	2.7	1.31	0.019	3.3	0.495	66.7	134.7	22.45	133.7
APM 36-08	1.735	1.7	0.084	1.9	0.004	7.5	0.04	0.663	6.4	0.871	157.5	180.7	5.65	
(migmatite)	2.896	1.7	0.147	1.8	0.004	4.5	0.03	0.408	4.5	0.812	156.5	192.7	7.13	
	0.980	1.8	0.051	2.1	0.003	8.7	0.06	0.281	6.3	0.799	147.7	184.8	7.35	
	1.768	1.7	0.080	1.9	0.003	5.2	0.04	0.393	4.5	0.859	171.9	200.1	6.46	
	0.555	1.9	0.029	2.3	0.002	7	0.06	0.293	4.6	0.891	142.7	160.2	5.19	
	0.511	1.8	0.030	2.3	0.003	5	0.11	0.198	4.7	0.862	129.9	150.7	5.18	
	4.793	1.7	0.208	1.8	0.013	3	0.06	0.775	4.6	0.926	179.8	194.1	5.07	181.8
APM 37-08	1.367	1.7	0.071	2.1	0.009	4.6	0.13	0.283	5.1	0.819	148.5	181.4	6.74	
(mica schist)	0.263	2	0.033	2.4	0.003	5.1	0.1	0.074	5.6	0.840	63.4	75.5	2.9	
	0.806	1.8	0.057	2	0.009	3.5	0.16	0.244	5.8	0.885	107.8	121.8	3.76	
	1.164	1.8	0.064	2	0.004	5	0.07	0.289	5.7	0.823	142.2	172.7	6.34	137.9
APM 48-08	2.203	1.7	0.081	2	0.011	4.2	0.13	0.714	4.8	0.799	201.6	252.2	9.77	
(granite)	2.467	1.7	0.113	1.9	0.012	3.2	0.1	0.633	5.3	0.894	166.9	186.7	5.38	
	4.698	1.7	0.165	1.9	0.017	3.5	0.1	1.128	4.9	0.856	214.6	250.7	8.02	
	5.598	1.7	0.172	1.8	0.022	2.8	0.13	0.898	5.4	0.884	246.3	278.7	8.16	
	7.677	1.7	0.255	1.8	0.023	2.7	0.09	1.180	5.3	0.892	230.7	258.6	7.38	245.4
APM 49-08	0.768	1.8	0.035	2.3	0.132	2.5	3.75	0.396	6.1	0.820	91.0	111.1	4.05	
(granite)	1.490	1.7	0.089	1.9	0.363	2.4	4.1	0.741	5.4	0.876	68.0	77.6	2.27	
	0.393	2	0.022	2.9	0.082	2.6	3.75	0.215	5.9	0.774	75.1	97.0	4.2	
	1.423	1.7	0.094	1.9	0.297	2.4	3.17	0.708	5.4	0.875	69.0	78.8	2.3	
	0.696	1.8	0.034	2.4	0.048	2.6	1.42	0.335	5.5	0.886	118.6	133.9	4.09	
	2.224	1.7	0.117	1.9	0.429	2.4	3.68	0.782	5.4	0.873	81.4	93.3	2.74	
	1.442	1.7	0.060	2	0.189	2.4	3.15	0.568	5.4	0.904	108.3	119.8	3.21	105.1

Carboniferous to Middle Permian times. An exception of this is given by samples APM 49-08, 34-08 and 33-08, which show initial cooling below the  $PRZ_Z$  in Carboniferous times, indicating an older thermal history of these samples.

The temperature regime for the apatite fission track partial-annealing zone (PAZ $_{\rm A}$   $\approx$ 110-90 °C) was passed in Middle Permian to Early Triassic times. The lower temperature boundary recorded by our data (PRZ $_{\rm A}$   $\approx$ 65 °C) was reached in late Permian to

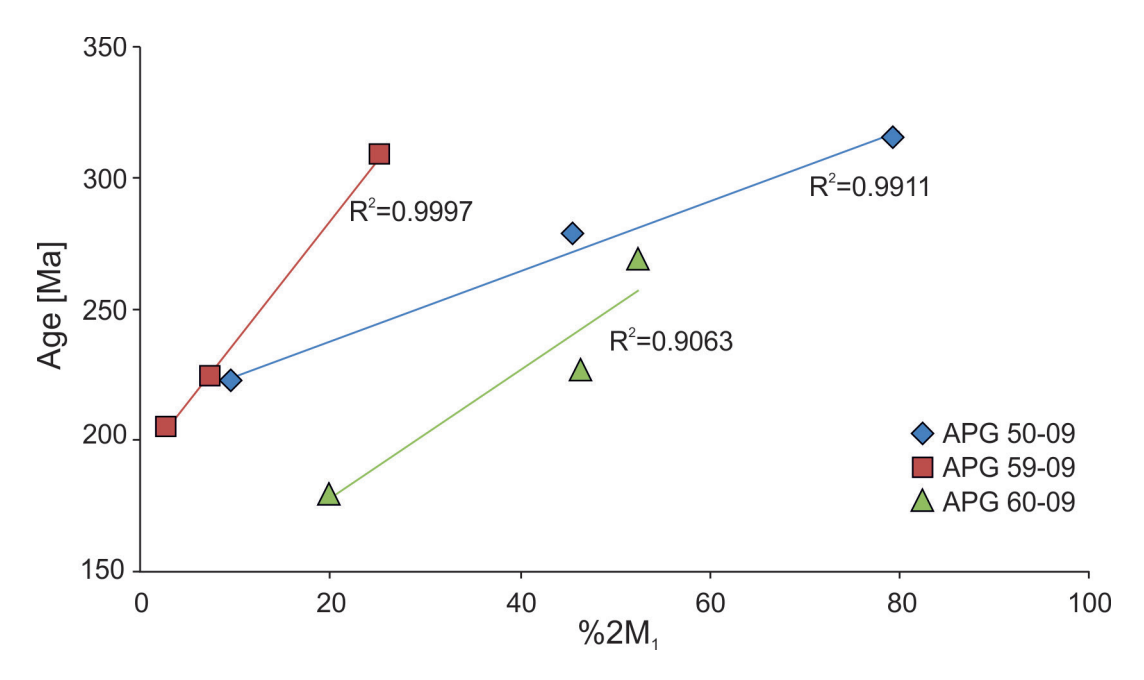


FIG. 9. K-Ar ages *versus* % 2M<sub>1</sub> illite content for three analyzed samples. Polytype composition was determined using XRD-methods. Plots show a coefficient of determination (R²) better than 0.9, confirming a clear linear relationship between age and 2M<sub>1</sub> polytype content. Based on this relationship, ages for hypothetical fractions consisting of 0% 2M<sub>1</sub> were calculated by linear extrapolation (see text for a detailed discussion).

Jurassic times, or even in the Cretaceous. We attribute this great span of cooling ages to a prolongation of very low cooling rates, as evident in all models (Fig. 10). Slow cooling and associated long-lasting residence time in the PRZ<sub>Z</sub>, PAZ<sub>A</sub> and PRZ<sub>A</sub> also led to a broad scattering of individual helium and fission-track ages (Fig. 7) and the development of a broad, unimodal fission track length distribution and distinct shortened tracks (Fig. 8). Assuming that these very slow cooling rates gave rise to low rates of surface exhumation (*i.e.*, limited erosion), suitable conditions were provided for the development of erosional surfaces during one or several regional planation events.

Based on model data, conservative calculations of cooling rates to temperatures around 175 °C (Figs. 10, 11) yields rates below 5 °C/Ma. For the temperature range of ca. 175 °C (PRZ<sub>Z</sub>) to ca. 65 °C (PRZ<sub>A</sub>), rates vary from around 2 °C/Ma to 10 °C/Ma. An exception of slow to moderate cooling rates is given by samples APM 34-08 and 49-08, which yield rates of 0.5 °C/Ma to 1.5 °C/Ma. These very low cooling rates, together with the observation of higher ages for cooling up to ca. 175 °C (see above), strongly indicate a different thermal history of samples

APM 34-08 and 49-08 in comparison to all other samples, at least for the cooling above the PRZ<sub>A</sub>. Results yielded by sample APM 34-08 are puzzling, whereas sample APM 49-08 is located at the boundary of a low relief area within the western Sierra de San Luis hillslope. Field studies have highlighted that the western range hillslope is a complex uplift scarp in the study area, composed by several morphotectonic domains bounded by fault zones (Costa, 1992; Costa et al., 1999). These geological evidences together with the mismatch of thermochronological data thus indicate that differential rates of exhumation and/or uplift resulted from segmentation and presence of several fault-bounded blocks (Fig. 12).

Very low cooling rates of <0.5 °C/Ma are calculated for all models in the temperature range of 65 °C to around 30 °C. Final cooling to the present day mean surface temperature of 17 °C (Müller, 1996) is less constrained by models but most likely in the range of 0.5 to 1.5 °C/Ma.

## 5.2. Timing of faulting constrained by K-Ar ages

Following the method suggested by Bense *et al.* (2014), we interpret the 100% 1M<sub>d</sub> end-member

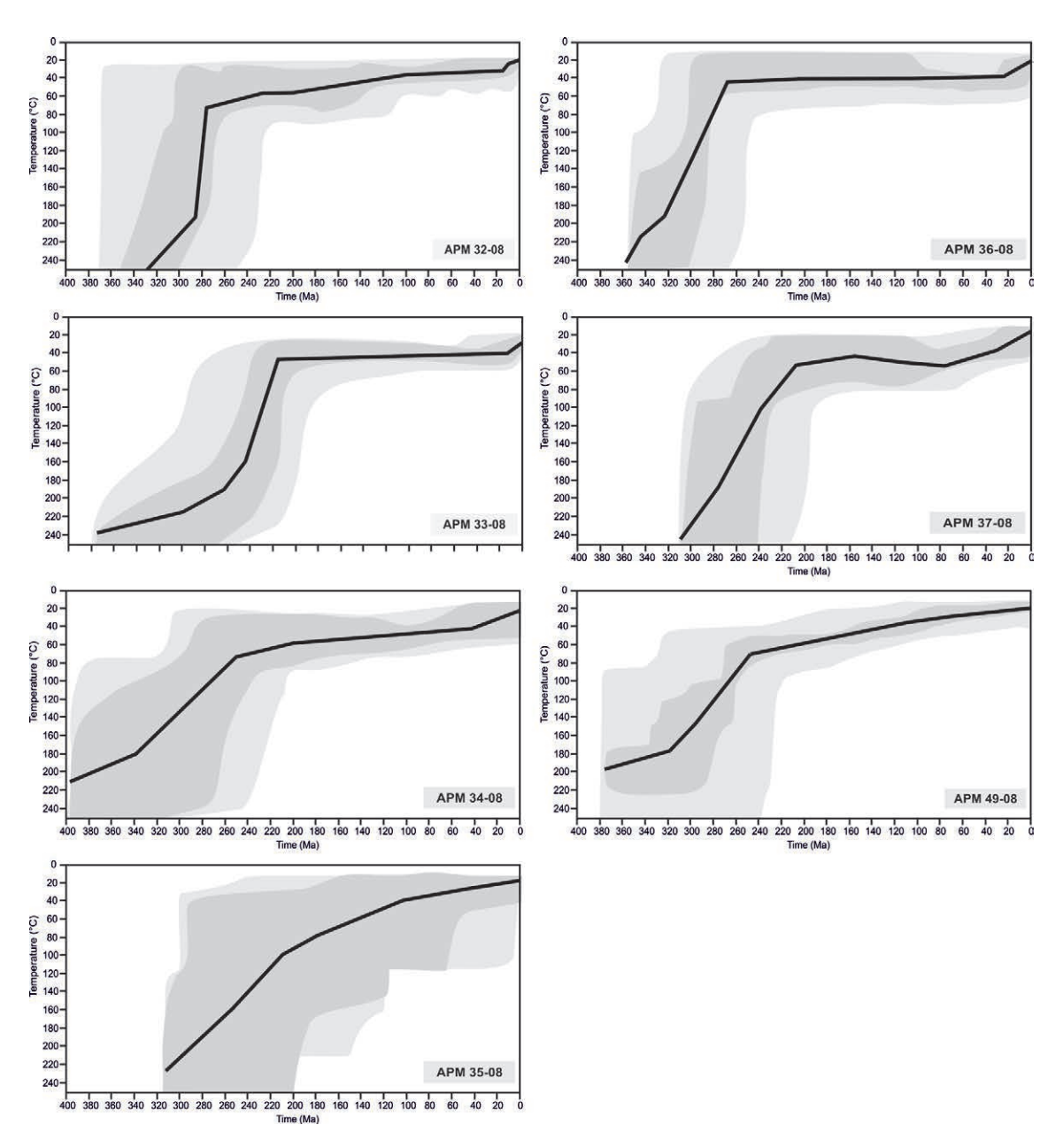


FIG. 10. Possible t-T paths for individual samples based on Fission track single grain ages and the confined track length distribution as well as the (U-Th)/He ages of apatite and zircon; light grey paths: acceptable fit, dark grey: good fit, black line: best fitting path. With exception of APM 35-08 all models are based on (U-Th)/He data from zircon and apatite and Apatite Fission track data. Model 35-08 is only based on (U-Th)/He data.

(mathematical age of an hypothetical sample consisting of 100% 1M illite, see above) age to best represent the age of the youngest deformational movement resulting in illite formation along sampled faults because the age-increasing influence of the "older" 2M<sub>1</sub> polytypes is eliminated. In turn, the

complementary  $2M_1$  end-member age may represent a) the oldest generation of neoformed illite, under retrograde (cooling) conditions (see Bense *et al.*, 2014) and/or b) the age of "detrital" muscovite, meaning crushed muscovite from the host rock (Fig. 13). Concerning the latter, the absence of

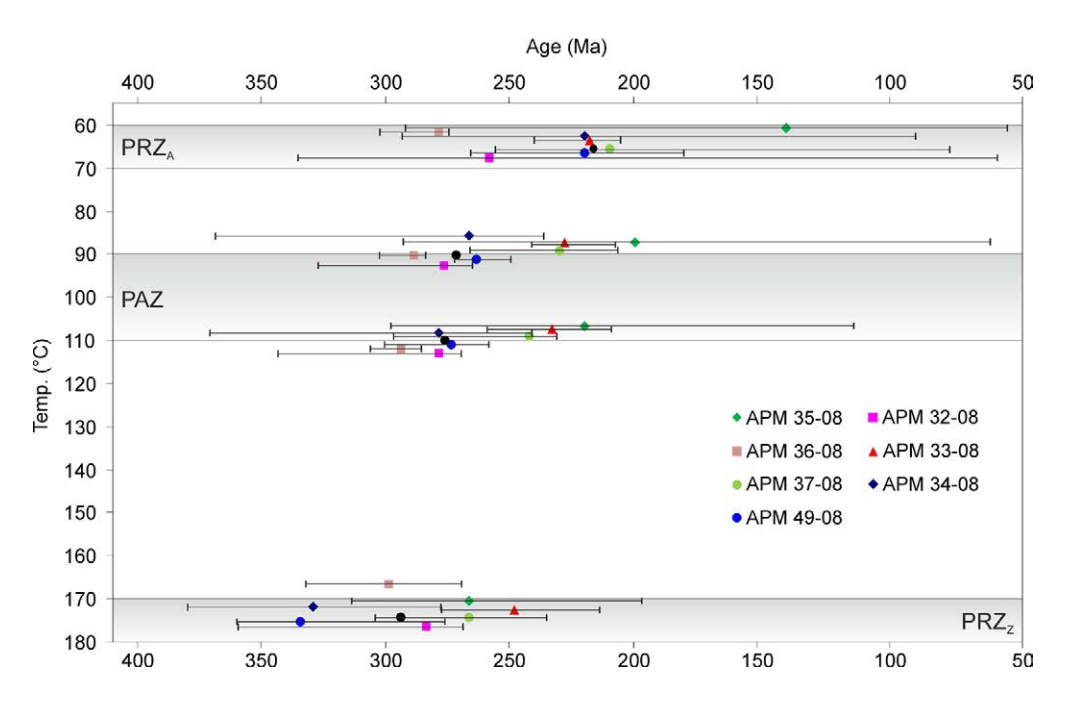


FIG. 11. Thermal history for the San Luis profile based on individual t-T paths presented in figure 10. Horizontal error bars decipher the range of good fits, the position of the marker represents position of best fit path (Fig. 10). For a better illustration the individual samples are exhibited at slightly different temperatures. The approximate temperature ranges of the Partial Retention Zone for zircon (PRZ<sub>2</sub>), the Partial Annealing Zone for apatite (PAZ<sub>A</sub>) as well as the Partial Retention Zone for apatite (PRZ<sub>A</sub>) are shown as grey bars. The high range in ages of sample APM 35-08 is due to lack of Apatite Fission Track data (Fig. 10).

extremely low KI-values (ca. 0.060  $\Delta$ °2 $\theta$ ) in mineral fine fractions indicates that a contamination by cataclastically crushed muscovite from the host rock is very unlikely.

If the 2M<sub>1</sub> illite age represents the onset of brittle deformation, it should always be younger than a K-Ar biotite cooling age from the same rock or nearby location (Fig. 4). Biotite shows a closure temperature around 300 °C (McDougall and Harrison, 1999) and can be interpreted to date the cooling of the basement close to brittle-ductile transition temperatures. Thus, biotite K-Ar ages represent cooling ages that predate the onset of brittle deformation and formation of illite in fault gouges (Fig. 4).

In the Nogolí region, K-Ar biotite ages from basement samples yield Carboniferous ages (345-328 Ma; Steenken *et al.*, 2008) and are older than illite fine-fraction ages. Except one sample, they overlap with extrapolated 100% 2M<sub>1</sub> illite ages within error.

Further constraint is given by K-Ar and Ar/Ar muscovite ages (Fig. 14), yielding Devonian ages (380-350 Ma; Sims *et al.*, 1998; Steenken *et al.*, 2008) and Carbonifeous K-Ar fine fraction ages (345-299 Ma;

Wemmer et al., 2011). The latter ages were taken from the San Luis Formation, represented by two belts of low-grade phyllites and quartz arenites, several kilometres to the north of the study area. The former mentioned muscovite ages are interpreted to represent the last mylonitization event caused by the Achalian Orogenic Cycle before brittle deformation started (Sims et al., 1998; Steenken et al., 2008), whereas K-Ar fine fraction ages from the San Luis Formation are interpreted to coincide with deformation under ductile/brittle transition conditions and the end of ductile deformation (Wemmer et al., 2011). All illite grain-size fraction ages presented here are younger or, in case of extrapolated 100% 2M, ages, overlap within error with K-Ar and Ar/Ar cooling ages, supporting our interpretation. Hence, the western Sierra de San Luis basement achieved depth/temperature levels below the brittle/ductile transition zone due to active deformation and exhumation during the latest Carboniferous/earliest Permian.

Illite-generating fault gouge activity along the sampled faults is interpreted to have ceased between 222 Ma and 173 Ma, as shown by the majority of the

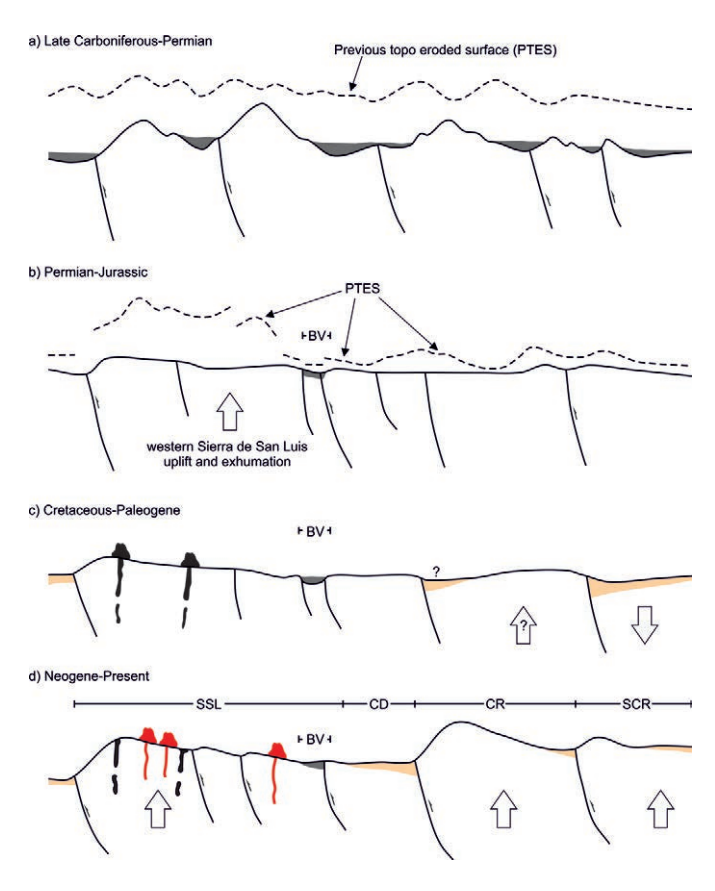


FIG. 12. Schematic exhumation model for the Sierra de San Luis and adjacent areas. See text for details (**BV**: Bajo de Véliz; **PTES**: Previous Topographic Eroded Surface; **SSL**: Sierra de San Luis; **CD**: Conlara Depression; **CR**: Comechingones range; **SCR**: Sierra Chica Range; white arrow indicating area affected by uplift or subsidence). For further details on the Sierra de Comechingones see Löbens *et al.* (2011).

<0.2 µm grain-size fractions as well as the calculated 100% 1M<sub>4</sub> illite fractions (Table 1). Only one sample (APG 60-09) shows a younger age for the calculated 100% 1M<sub>d</sub> fraction of 119 Ma. This comparatively young age might be related to an extrapolation error resulting from its-compared to the other samples-low 1  $M_d$  illite content in the <0.2  $\mu$ m fraction (Table 1). The youngest age documented by fault gouge dating must not be considered to represent the cessation of fault activity but to represent the last illite-forming event and, thus, the cooling of the fault block below illite-forming temperatures (approximately between 75-110 °C; e.g., Hamilton et al., 1992; Fig. 4). Cooling below the illite-forming temperatures is constrained by AFT and AHe ages (Tables 4 and 5). The youngest illite must overlap with the apatite fission track ages (representing cooling below 110 °C), whereas the AHe ages (representing cooling below 60 °C) must

always be younger than the K-Ar illite ages (Fig. 4). This can indeed be observed for all analysed samples (Fig. 14; Tables 1-3, see also Bense *et al.*, 2014).

# 5.3. Implications for the evolution of the Sierra de San Luis

The onset of brittle deformation in the western part of the present-day Sierra de San Luis during the Late Devonian to Early Carboniferous, suggest that this rock massif was already emplaced at shallow crustal levels by that time. Although there are no landscape remains of this evolutionary stage, it is suggested that surface uplift of the area related to the present day range configuration, driven by faulted blocks uplift, started during that time. This crustal mobility may be related with the development of shear zones under brittle-ductile conditions in several parts of the range

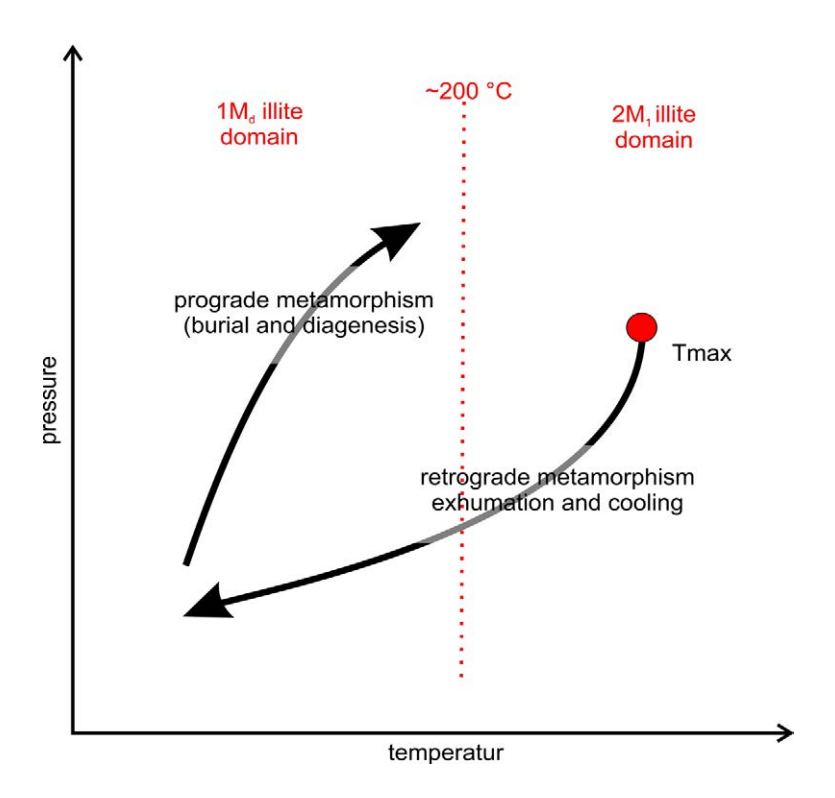


FIG. 13. Illite polytypism in fault gouges in relation to temperature conditions during prograde and retrograde metamorphism. Generally when interpreting illite polytypism from fault gouges prograde metamorphic conditions are assumed. As a consequence  $2M_1$  illite is considered a detrital component derived from source rock, because temperature conditions in fault zone are regarded as insufficient for the development of  $2M_1$  illite (*i.e.*, ca. 200 °C). However, sufficient temperature for  $2M_1$  illite development can be ensured when the host rock experienced brittle deformation during regional cooling and passage of epizonal conditions during retrograde metamorphism (Bense *et al.*, 2014). Thus, in case of non-sedimentary host-rocks, the  $2M_1$  illite must not be excluded from consideration as meaningful fault gouge age.

during the Achalian Cycle, whose effects according to Sims *et al.* (1997, 1998) can be documented up to 355 Ma. Such significant episode of exhumation and uplift may also be linked to the collision of the Chilenia exotic terrane at the proto-pacific margin of Gondwana (Chanic orogeny) during the late Devonian (Ramos, 1988; Mpodozis and Ramos, 1989; Davis *et al.*, 1999; Willner *et al.*, 2011).

During the Carboniferous to the Early Permian (Fig.12a), a mountainous landscape developed as suggested by Jordan *et al.* (1989), associated with the down-wearing of the Early Carboniferous topography. Aiming to reconstruct possible evolutionary paths, this primary landscape is represented as an imaginary primary topographic enveloping surface (PTES; Fig. 12).

Several intermountain basins of unknown extent and dimensions developed during this phase, which record fluvial-lacustrine sedimentation (*e.g.*, fault-bounded depressions of Bajo de Véliz and La

Estanzuela; Hünicken *et al.*, 1981; Limarino and Spalletti, 2006; Chernicoff and Zappettini, 2007). These depocenters were part of the eastern Paganzo basin, which contains basement-derived clasts with provenance mainly from the east, indicating surface uplift of the easternmost Sierras Pampeanas to some extent during basin development (López-Gamundí *et al.*, 1994; Chernicoff and Zappettini, 2007). A similar situation with a Carboniferous landscape carved into older rocks and covered or filled by fluvial sediments was documented in the Sierra de Chepes (La Rioja province) by Enkelmann *et al.*, 2014).

Based on thermal modelling results, the middle Permian to early Jurassic can be identified as main exhumation phase, comprising around 40-50% of the total exhumation recorded by thermochronological data and can be ascribed to the effects of the San Rafael orogeny and the subsequent extensional orogenic

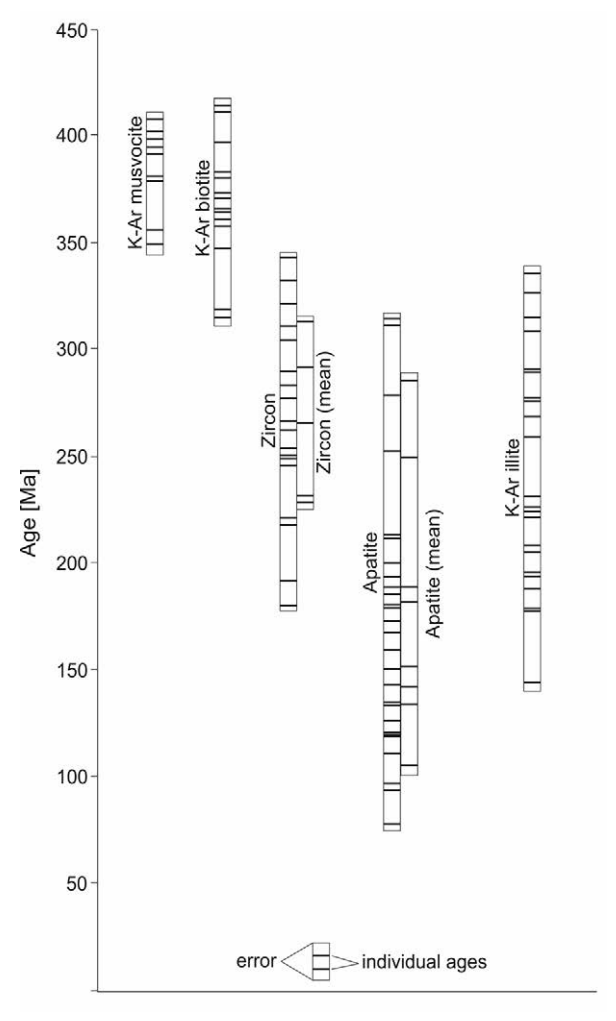


FIG. 14. Compilation of available geochronological data of the study area in comparison to K-Ar illite ages from fault gouges. For better view geochronometers are displayed in the x-axis. K-Ar muscovite and biotite data are taken from Steenken *et al.* (2008) and Wemmer *et al.* (2011). Black lines indicate individual ages, bars indicate overlapping error of individual ages.

collapse (Ramos, 1988; Mpodozis and Ramos, 1989; Kleiman and Japas, 2009) in the study range. Upper Paleozoic to Jurassic exhumation was also reported for the Sierras de Córdoba, Sierra de Pie de Palo and Sierra de Aconquija (Löbens *et al.*, 2013a, b; Richardson *et al.*, 2013). In combination with the fact that Gondwanic sediments were preserved in the Bajo de Véliz region, data presented herein evidence a differential exhumation in the Sierra de San Luis. While the eastern range area (Bajo de Véliz) was exhumed to a surface or a near-surface position, allowing interaction with surficial processes, the western part (study area) was at least at several kilometres below the present surface by that time. This fact suggests that

exhumation related to differential block movement driven by faulting was active at least during Permian times. A mountainous landscape probably prevailed by then in this region, whereas planation processes, which led to the present-day erosional surfaces and flat topography, might not start before the Late Permian at the western San Luis range (Fig. 12b).

Triassic exhumation and deformation is recorded by K-Ar fault gouge and thermochronological data, resulting from rifting in the Andean foreland during extension (Kay *et al.*, 1991; Giambiagi *et al.*, 2011; Sato *et al.*, 2015). Coeval volcaniclastic rocks are recorded in the Sierra de Varela area, *ca.* 100 km to the south of the Sierra de San Luis with a half-graben

array, though the timing of rifting is not well known (Costa *et al.*, 1998b).

Although final exhumation to the surface level is not well constrained by the data, thermal modelling (Fig. 11, Tables 4 and 5) indicates that cooling below temperatures of about 60 °C for the study area did not occur up to the Upper Cretaceous (Fig. 12c). On the other hand, thermal modelling shows cooling below temperatures of 50-30 °C for all samples during the Cenozoic (Fig. 10). Considering a surface temperature of 17 °C (Müller, 1996), Cenozoic cooling rates between 0.2-0.5 °C/Ma can be estimated for the study area. This may be equivalent to a total Cenozoic exhumation of 0.6-1.8 km, if a geothermal gradient of 18 to 23 °C/km is assumed based on recent estimations (Dávila and Carter, 2013). Even if a lower geothermal gradient is considered, as indicated by Collo et al. (2011; 2015) for the Bermejo and Vinchina basins (~400 km to the northwest of the study area), maximum possible Cenozoic exhumation is constrained at 0.8-2 km. If the exhumation since the Cretaceous would have exceeded this difference, samples from the footslope area of the range must yield younger, reset ages. Additionally, this would be represented by a break in the slope in the age-elevation plot (Gleadow and Fitzgerald, 1987).

Thermochronological data indicate no significant/ measurable exhumation after Cretaceous times, suggesting that sampled rocks were already at or near surface by the Cretaceous or even before. Upper Cretaceous basaltic rocks emplaced near or at the surface further indicate that at least during the late Cretaceous the upper parts of the Sierra de San Luis were already exposed as a positive area prone to denudation processes (López and Solá, 1981). Following England and Molnar (1990) definitions, Cenozoic morphotectonic evolution might thus result from surface uplift of exhumed surfaces and/ or subsidence rather than from exhumation. There is no doubt that range uplift leading to the present day landscape occurred during the Neogene, due to an eastward migration of the locus of deformation (Ramos, 1988; Costa, 1992; Costa and Vita-Finzi, 1996; Costa et al., 2001b; Ramos et al., 2002). As a result, morphogenetic processes related to base level adjustment of fluvial systems seem to have dominated the present day morphology of the western slope (Costa, 1992). Evidences of a significant landscape rejuvenation starting in the

Neogene are suggested by preservation of wide planation surfaces atop the range; landforms association along the western hillslope and piedmont indicating significant channel downcutting; thrusting of Neogene and Quaternary strata by the range bounding San Luis Fault System (Costa, 1992; Costa *et al.*, 1999, 2000, 2001b).

K-Ar fault gouge ages do not shed light on the crustal stress regime, but constrain the onset of brittle deformation in the western part of the range to the Late Carboniferous/Early Permian. This time span matches with regional tectonic processes such as the development of the Paganzo Basin (Limarino and Spalletti, 2006; Gulbranson et al., 2010) and the San Rafael Orogeny (Ramos, 1988; Kleiman and Japas, 2009; Geuna et al., 2010; Japas et al., 2013). Active deformation during basin development was accompanied by exhumation of the study area, as indicated by K-Ar fine fraction data from Wemmer et al. (2011) and thermochronological data presented here (Figs. 7, 10). Ongoing Permian deformation and associated exhumation is recorded by K-Ar fault gouge and thermochronological data (Figs. 5, 7, 10), and might be related to basin inversion associated with the San Rafael Orogeny (Ramos, 1988; Kleiman and Japas, 2009; Geuna et al., 2010; Japas *et al.*, 2013).

Carboniferous exhumation and uplift related to active deformation was also reported for the Sierra de Chepes (Fig. 1; Enkelmann *et al.*, 2014), whereas coeval fault activity was recognized for the Sierras de Córdoba (Whitmeyer, 2008) and the Sierra de Comechingones (Löbens *et al.*, 2011) based on Ar/Ar pseudotachyllite and K-Ar fault gouge data, respectively. Permian exhumation and deformation, in turn, is also recorded in other areas of the Sierras Pampeanas (Coughlin *et al.*, 1998; Bense *et al.*, 2013, 2014; Sato *et al.*, 2015).

#### 5.4. Development of planation surfaces

It is assumed that regional tectonic unrest during the Triassic did not favour the development of planation surfaces of regional significance. In addition, a Triassic emergence of the sampled area is not supported by AHe ages, which yield predominantly Jurassic and Cretaceous ages (see above).

During Late Jurassic-Early Cretaceous times, rifting took place east and west of the Sierra de San Luis (Gordillo and Lencinas, 1967, 1979;

González and Toselli, 1973; Yrigoyen, 1975; Schmidt et al., 1995). As a consequence, regional planation processes took place most likely during the Lower-Middle Jurassic and/or during the Late Cretaceous, although data presented here cannot discriminate if major erosion surfaces are diachronous in time, as suggested by Carignano (1999) and Rabassa et al. (2010, 2014). AHe ages indicate that both time intervals contributed to the exhumation of the sampled area. Samples from higher elevations in the eastern part of the study area show predominantly Jurassic ages (Table 5) and were probably also emerged during this time. Instead, samples representing the footslope area of the western range passed through PRZ conditions in middle Cretaceous times (AHe mean age of 105 Ma, see Table 5). Whether or not emergence occurred during this time cannot be concluded from the data.

Further constraints comprise basalts emplaced at higher altitudes in the Sierra de San Luis to the northeast of the study area (Fig. 12c), which yield K-Ar ages of 83±6 Ma (López and Solá, 1981). The effusive character of the dated basalts is unclear because no robust field evidence for effusion above erosional surface has been reported and they might alternatively comprise a subvolcanic intrusion. If these basalts were emplaced atop the erosional surface, the emergence and formation of the erosional surface should be considered to be older than 83±5.85 Ma. In this case, final exhumation to surface of the present day top of the Sierra de San Luis occurred between the Jurassic and Upper Cretaceous. If, in contrast, the basalts represent subvolcanic bodies with no relationship to a paleosurface, no further interpretations regarding the final exhumation can be made with available data.

Ages of basaltic rocks are in contrast to AHe single grain ages of the lowermost sample from the western footslope (APM 49-08), which show a minimum age for passage through the PRZ<sub>A</sub> of 72 Ma (Table 5), coinciding with a depth of about 2.4 km (considering a geothermal gradient of 25 °C/km). This favours the idea of diachronous development of the erosional surfaces in this part of the range due to differential block uplift, with an older surface on top of the range (>83 Ma) and a younger erosional surface (<72 Ma) barely developed in secondary blocks located at the main western range hillslope.

#### 6. Conclusions

Exhumation of the section of the Sierra de San Luis studied here started during Carboniferous times. The middle Permian and Triassic to early Jurassic can be identified as the main exhumation phase, comprising around 40-50% of the total exhumation recorded by the applied thermochronological methods. Cooling rates varied between 2-10 °C/Ma during the Permian and Triassic periods. Post-Triassic cooling yields lower rates of 0.5-1.5 °C/km. Generally, exhumation took place differentially across the range, propagating from east to the west.

K-Ar fault gouge and thermochronological data reveal that crustal deformation and associated exhumation during the main exhumation phase were related to main tectonic processes. The Carboniferous evolution could be related to the development of the southeasternmost Paganzo Basin, whereas Permian exhumation is here associated with basin inversion during the San Rafael Orogeny. Crustal extension and rifting, in turn, gave rise to Triassic deformation and exhumation.

Because the range already cooled to near surface temperatures in Jurassic to Cretaceous times, thermochronological data give no explicit evidence for any Cenozoic exhumation, although Neogene range uplift is evident by geological and geomorphological data. Relative steady conditions persisted in the area nowadays, documented by planation surface remnants since the Cretaceous, and Apatite ages, as samples passed through the PRZ predominantly in Jurassic to Cretaceous times. This episode probably comprises the period when most of the remaining erosional surfaces were developed. The final structural relief and present topography of the Sierra de San Luis has been achieved as a result of Neogene regional crustal shortening and consequent differential uplift of surfaces which were already exhumed during Late Paleozoic and predominantly Mesozoic times.

## Acknowledgments

This research project is financed by the German Science Foundation (DFG project SI 438/31-1). The authors gratefully thank the constructive review by L. Giambiagi. We are also grateful for the careful sample preparation made by A. Süssenberger and the help of E. Ahumada and M. López de Luchi, alleviating the stay in Argentina, as well as A. Steenken and J.A. Palavecino

assisting in the field. Field work done by F. Bense was financially supported by the DAAD (project number D/08/48018).

#### References

- Baile, S.W. 1966. The status of clay mineral structures. *In* Clays and Clay Minerals 14 (1): 1-23. doi: 10.1346/CCMN.1966.0140101.
- Baldwin, S.L.; Lister, G.S. 1998. Thermochronology of the South Cyclades Shear Zone, Ios, Greece: effects of ductile shear in the argon partial retention zone. Journal of Geophysical Research 103 (B4): 7315-7336. doi:10.1029/97JB03106.
- Bense, F.A.; Löbens, S.; Dunkl, I.; Wemmer, K.; Siegesmund, S. 2013. Is the exhumation of the Sierras Pampeanas only related to Neogene flat-slab subduction? Implications from a multi-thermochronological approach. Journal of South American Earth Sciences 48: 123-144.
- Bense, F.A.; Wemmer, K.; Löbens, S.; Siegesmund, S. 2014. Fault gouge analyses: K-Ar illite dating, clay mineralogy and tectonic significance-a study from the Sierras Pampeanas, Argentina. International Journal Earth Sciences 103: 189-218.
- Caillere, S.; Henin, S.; Rautureau, M. 1982. Mineralogie des Argiles. Edité par Masson, París: 184 p.
- Carignano, C. 1999. Late Pleistocene to recent climate change in Córdoba Province, Argentina: Geomorphological evidence. Quaternary International 57-58 (1): 117-34. doi:10.1016/S1040-6182(98)00054-8.
- Chernicoff, C.J.; Zappettini, E.O. 2007. La cuenca neopaleozoica de Arizona, sudeste de San Luis, Argentina: prolongación austral de la cuenca de Paganzo. Revista de la Asociación Geológica Argentina 62: 321-324.
- Clauer, N.; Srodon, J.; Francu, J.; Sucha, A. 1997. K-Ar dating of illite fundamental particles separated from illite-smectite. Clays and Clay Minerals 32: 181-196.
- Collo, G.; Dávila, F.M.; Nóbile, J.; Astini, R.A.; Gehrels, G. 2011. Clay mineralogy and thermal history of the Neogene Vinchina Basin, central Andes of Argentina: Analysis of factors controlling the heating conditions. Tectonics 30 (4): TC4012. doi: 10.1029/2010TC002841.
- Collo, G.; Dávila, F.M.; Teixeira, W.; Nóbile, J.C.; Sant'Anna, L.G.; Carter, A. 2015. Isotopic and thermochronologic evidence of extremely cold lithosphere associated with a slab flattening in the Central Andes of Argentina. Basin Research. doi: 10.1111/bre.12163.

- Cordani, U.; Milani, E.J.; Thomaz Filho, A.; Campos, D.A. 2001. Tectonic Evolution of South America. Brazilian Academy of Sciences: 854 p. Río de Janeiro.
- Costa, C.H. 1992. Neotectónica del sur de la Sierra de San Luis. Ph.D. Thesis (Unpublished), Universidad Nacional de San Luis: 320 p.
- Costa, C.H.; Vita-Finzi, C. 1996. Late Holocene Faulting in the southeast Sierras Pampeanas of Argentina. Geology 24: 1127-1130.
- Costa, C.H. 1999. Rasgos estructurales del territorio argentino, tectónica cuaternaria en las Sierras Pampeanas. Instituto de Geología y Recursos Minerales-Servicio Geológico Minero Argentino (SEGEMAR), Geología Argentina, Anales 29: 779-784.
- Costa, C.H.; Ortiz Suárez, A.; Gardini, C.; Chiesa, J.; Ojeda, G.; Strasser, E.; Escayola, M.; Kraemer, P.; Ulacco, H.; Morla, P.; Almandoz, G.; Coniglio, J. 1998a. Hoja Geológica 3366-II, Santa Rosa, provincias de San Luis y Córdoba, escala 1:250.000. Servicio Geológico Minero Argentino (SEGEMAR), Boletín 373, CD Rom.
- Costa, C.H.; Gardini, C.E.; Schmidt, C.J.; Guerstein, P. G. 1998b. Dataciones <sup>40</sup>Ar/<sup>39</sup>Ar y rasgos estructurales de la Formación Cerro Varela (Triásico), provincia de San Luis. Revista de la Asociación Geológica Argentina 53 (2): 282-285.
- Costa, C.H.; Giaccardi, A.D.; González Díaz, E.F. 1999. Palaeolandsurfaces and neotectonic analysis in the southern Sierras Pampeanas, Argentina. *In* Uplift, erosion and stability: Perspectives on long-term landscape development (Smith, B.J.; Whalley, B.; Warke, P.A.; editors). Geological Society of London, Special Publications 162: 229-238. doi:10.1144/GSL. SP.1999.162.01.18.
- Costa, C.H.; Gardini, C.E.; Ortiz Suárez, A.; Chiesa, J.; Ojeda, G.; Rivarola, D.; Strasser, E.; Morla, P.; Ulaco, J.; Tognelli, G.; Carugno Durán, A.; Vincinguerra, H.; Salas, D. 2001a. Hoja Geológica 3366-I San Francisco del Monte de Oro. Servicio Geológico Minero Argentino (SEGEMAR), Boletín 278: 82 p.
- Costa, C.H.; Murillo, V.M.; Sagripanti, G.L.; Gardini, C.E. 2001b. Quaternary intraplate deformation in the southeastern Sierras Pampeanas, Argentina. Journal of Seismology 5: 399-409.
- Costa, C.; Ortiz Suárez, R.; Miró, J.; Chiesa, C.; Gardini, A.;
  Carugno Durán, G.; Ojeda, P.; Guerstein, G.; Tognelli,
  P.; Morla y Edgardo Strasser, 2005. Hoja Geológica
  3366-IV, Villa Mercedes, Provincias de San Luis
  y Córdoba. Servicio Geológico Minero Argentino
  (SEGEMAR), Boletín 348: 100 p.

- Coughlin, T.J.; O'Sullivan, P.B.; Kohn, B.P.; Holcombe, R.J. 1998. Apatite fission-track thermochronology of the Sierras Pampeanas, central western Argentina: Implications for the mechanism of plateau uplift in the Andes. Geology 26: 999-1002.
- Criado, R. 1972. El cinturón movil Mendocino-Pampeano. In Geología Regional Argentina (Turner, J.; editor). Academia Nacional de Ciencias: 297-303. Córdoba.
- Criado Roque, P.; Mombrú, C.; Ramos, V.A.; Yrigoyen, M. 1981. Estructura e interpretación tectónica. Geología de la Provincia de San Luis. *In* Congreso Geológico Argentino, No. 8, Relatorio: 155-192. San Luis.
- Dávila, F.M.; Carter, A. 2013. Exhumation history of the Andean broken foreland revisited. Geology 41: 443-446.
- Davis, J.S.; Roeske, S.M.; McClelland, W.C.; Snee, L.W. 1999. Closing the ocean between the Precordillera terrane and Chilenia: Early Devonian ophiolite emplacement and deformation in the southwest Precordillera. Geological Society of America, Special Papers 336: 115-138.
- Dollase, W. 1986. Correction of intensities for preferred orientation in powder diffractometry: Applications of the March mode. Journal of Applied Crystallography 19: 267-272.
- Donelick, R.A.; Ketcham, R.A.; Carlson, W.D. 1999.Variability of apatite fission-track annealing kinetics:II. Crystallographic orientation effects. American Mineralogist 84: 1224-1234.
- Dunkl, I. 2002. TRACKKEY: a Windows program for calculating and graphical presentation of fission-track data. Computational Geosciences 28: 3-12.
- Dunkl, I.; Mikes, T.; Simon, K.; Eynatten, H. von. 2008. Brief introduction to the Windows program Pepita: data visualization, and reduction, outlier rejection, calculation of trace element ratios and concentrations from LA-ICPMS data. Mineralogical Association of Canada, Short Course 40: 334-340.
- Enkelmann, E.; Ridgway, K.D.; Carignano, C.; Linnemann, U. 2014. A thermochronometric view into an ancient landscape: Tectonic setting, development, and inversion of the Paleozoic eastern Paganzo basin, Argentina. Lithosphere 6: 93-107.
- England, P.; Molnar, P. 1990. Surface uplift, uplift of rocks, and exhumation of rocks. Geology 18 (12): 1173-1177.
- Farley, K.A.; Wolf, R.A. 1996. The effects of long alphastopping distances on (U-Th)/He ages. Geochimica et Cosmochimica Acta 60 (21): 4223-4229.
- Fitzgerald, P.G.; Baldwin, S.L.; Webb, L.E.; O'Sullivan, P.B. 2006. Interpretation of (U-Th)/He single grain

- ages from slowly cooled crustal terranes: A case study from the Transantarctic Mountains of southern Victoria Land. Chemical Geology 225 (1-2): 91-120. doi: 10.1016/j.chemgeo.2005.09.001.
- Friedrich, D. 1991. Eine neue Methode zur Bestimmung der Illit-Kristallinität mit Hilfe digitaler Meesswerterfassung. Diploma Thesis (Unpublished), Georg-August-Universität Göttingen: 63 p.
- Fuhrmann, U.; Lippolt, H.J.; Hess, J.C. 1987. Examination of some proposed K-Ar standards: <sup>40</sup>Ar/<sup>39</sup>Ar analyses and conventional K-Ar data. Chemical Geology 66: 41-51
- Galbraith, R.F.; Laslett, G.M. 1993. Statistical models for mixed fission track ages. Nuclear Tracks and Radiation Measurements 21: 459-470.
- Geuna, S.E.; Escosteguy, L.D.; Limarino, C.O. 2010. Paleomagnetism of the Carboniferous-Permian Patquía Formation, Paganzo basin, Argentina: implications for the apparent polar wonder path for South America and Gondwana during the Late Palaeozoic. Geologica Acta 8: 33-397.
- Gharrabi, M.; Velde, B.; Sagon, J. 1998. The transformation of illite to muscovite in pelitic rocks: contraints from X-ray diffraction. Clays and Clay Minerals 46 (1): 79-88. doi: 10.1346/CCMN.1998.0460109.
- Giambiagi, L.; Mescua, J.; Bechis, F.; Martínez, A.; Folguera, A. 2011. Pre-Andean deformation of the Precordillera southern sector, southern Central Andes. Geosphere 7: 219-239.
- Gleadow, A.J.W. 1981. Fission-track dating methods: what are the real alternatives. Nuclear Tracks and Radiation Measurements 5: 3-14.
- Gleadow, A.J.; Fitzgerald, P.G. 1987. Uplift history and structure of the Transantarctic Mountains: new evidence from fission track dating of basement apatites in the Dry Valley area, southern Victoria Land. Earth and Planetary Science Letters 82: 1-14.
- González Bonorino, F. 1950. Algunos problemas geológicos de las Sierras Pampeanas. Revista de la Asociación Geológica Argentina 5: 81-110.
- González Díaz, E. 1981. Geomorfología. Geología de la provincia de San Luis (Yrigoyen, M.; editor). *In* Congreso Geológico Argentino, No. 8, Actas: 193-236. Buenos Aires.
- González, R.E.; Toselli, A.J. 1973. Las rocas efusivas básicas de la Sierra de Las Quijadas al oeste de Hualtarán, Provincia de San Luis. Acta Geológica Lilloana 12: 89-104.
- González, P.D.; Sato, A.M.; Llambías, E.J.; Basei, M.A.S.; Vlach, S.R.F. 2004. Early Paleozoic structural and

- metamorphic evolution of Western Sierra de San Luis (Argentina), in relation to Cuyania accretion. Gondwana Research 7: 1157-1170.
- Gordillo, C.E.; Lencinas, A. 1967. Geología y petrología del extremo norte de la Sierra de Los Cóndores, Córdoba. Boletín de la Academia Nacional de Ciencias, Córdoba 46: 73-108.
- Gordillo, C.E.; Lencinas, A. 1979. Sierras Pampeanas de Córdoba y San Luis. *In* Simposio de Geología Regional Argentina, No. 2. Academia Nacional de Ciencias, Córdoba: 577-650. Córdoba.
- Grathoff, G.H.; Moore, D.M. 1996. Illite polytype quantification using Wildfire calculated X-ray diffraction patterns. Clays and Clay Minerals 44 (6): 835-842.
- Grathoff, G.H.; Moore, D.M.; Hay, R.L.; Wemmer, K. 1998. Illite Polytype Quantification and K-Ar Dating of Paleozoic Shales: A Technique to Quantify Diagenetic and Detrital Illite. *In* Shales and Mudstones II. Petrography, Petrophysics, Geochemistry, and Economic Geology, E. Schweizerbart'sche Verlagsbuchhandlung (Nägele u Obermiller): 161-175. Stuttgart.
- Gulbranson, E.L.; Montañez, I.P.; Schmitz, M.D.; Limarino, C.O.; Isbell, J.L.; Marenssi, S.A.; Crowley, J.L. 2010. High-precision U-Pb calibration of Carboniferous glaciation and climate history, Paganzo Group, NW Argentina. Geological Society of America, Bulletin 122: 1480-1498.
- Haines, S.H.; van der Pluijm, B.A. 2008. Clay quantification and Ar/Ar dating of synthetic and natural gouge: Application to the Miocene Sierra Mazatán detachment fault, Sonora, Mexico. Journal of Structural Geology 30 (4): 525-538. doi:10.1016/j.jsg.2007.11.012.
- Hamilton, P.J.; Giles, M.R.; Ainsworth, P. 1992. K-Ar dating of illites in Brent Group reservoirs: a regional perspective. *In* Geology of the Brent Group (Morton, A.C.; editor). Geological Society, Special Publications 61: 377-400. London.
- Hess, J.C.; Lippolt, H.J. 1994. Compilation of K-Ar measurements on HD-B1 standard biotite; 1994 status report. *In Phanerozoic Time Scale* (Odin, G.S.; editor), Bulletin de Liaison et d'information: 19-23. Paris.
- Hourigan, J.K.; Reiners, P.W.; Brandon, M.T. 2005. U-Th zonation-dependent alpha-ejection in (U-Th)/He chronometry. Geochimica et Cosmochimica Acta 69 (13): 3349-3365.
- Hünicken, M.A.; Azcuy, C.L.; Pensa, M.V. 1981. Sedimentitas Paleozoicas. *In Congreso Geológico Argentino*, No. 8, Relatorio: 55-77.

- Hunziker, J.C.; Frey, M.; Clauer, N.; Dallmeyer, R.D. 1986.

  The evolution of the illite to muscovite: mineralogical and isotopic data from the Glarus Alps, Switzerland.

  Contributions to Mineralogy and Petrology 92: 157-180.
- Hurford, A.J.; Green, P.F. 1983. The zeta age calibration of fission-track dating. Chemical Geology 41: 285-317.
- Hurford, A.J.; Hammerschmidt, K. 1985. <sup>40</sup>Ar/<sup>39</sup>Ar and K-Ar dating of the Bishop and Fish Canyon Tuffs: Calibration of ages for fission-track dating standards. Chemical Geology 58: 23-32.
- Jaboyedoff, M.; Kübler, B.; Sartori, M. 2000. Basis for meaningful illite crystallinity measurements: an example from the Swiss Prealps. Schweizerische mineralogische und petrographische Mitteilungen (80): 75-83.
- Jaboyedoff, M.; Bussy, F.; Kübler, B.; Thelin, P. 2001. Illite "crystallinity" revisited. Clays and Clay Minerals 49 (2): 156-167.
- Japas, M.S.; Rubinstein, N.A.; Kleiman, L.E. 2013. Strain fabric analysis applied to hydrothermal ore deposits emplaced during changing geodynamical conditions (Infiernillo and Las Picazas, San Rafael Massif, Argentina). Ore Geology Reviews 53: 357-372.
- Jordan, T.E.; Allmendinger, R.W. 1986. The Sierras Pampeanas of Argentina: A modern analogue of Rockey Mountain foreland deformation. American Journal of Science 286: 737-764.
- Jordan, T.E.; Isacks, B.L.; Allmendinger, R.W.; Brewer, J.A.; Ramos, V.A.; Ando, C.J. 1983. Andean tectonics related to geometry of subducted Nazca plate. Geological Society of America, Bulletin 94 (3): 341-361.
- Jordan, T.E.; Zeitler, P.; Ramos, V.A.; Gleadow, A.J. 1989.
  Thermochronometric data on the development of the basement peneplain in the Sierras Pampeanas, Argentina. Journal of South American Earth Sciences 2 (3): 207-222.
- Kay, S.M.; Abruzzi, J.M. 1996. Magmatic evidence for Neogene lithospheric evolution of the central Andean "flat-slab" between 30°S and 32°S. Tectonophysics 259: 15-28.
- Kay, S.M.; Mpodozis, C.; Ramos, V.A.; Munizaga, F. 1991. Magma source variations for mid-late Tertiary magmatic rocks associated with a shallowing subduction zone and thickenung crust in the Central Andes (28-33°S). *In* Andean Magmatism and its Tectonic Setting (Harmon, R.S.; Rapela, C.W.; editors). Geological Society of America, Special Paper 26: 113-137.
- Ketcham, R.A. 2005. Forward and inverse modelling of low-temperature thermochronometry data. Reviews in Mineralogy and Geochemistry 58: 275-314.

- Ketcham, R.A.; Donelick, R.A.; Carlson, W.D. 1999. Variability of apatite fission-track annealing kinetics: III. Extrapolation to geological time scales. American Mineralogist 84: 1235-1255.
- Kleiman, L.E.; Japas, M.S. 2009. The Choiyoi volcanic province at 34°S-36°S (San Rafael, Mendoza, Argentina): Implications for the Late Palaeozoic evolution of the southwestern margin of Gondwana. Tectonophysics 473 (3-4): 283-299. doi:10.1016/j. tecto.2009.02.046.
- Kralik, M.; Klima, M.; Riedmüller, G. 1987. Dating fault gouges. Nature 327: 315-317.
- Kübler, B. 1964. Les argiles indicateurs de métamorphisme. Revue de l'Institute Français du Petrolé 19: 1093-1112.
- Kübler, B. 1967. La cristallinité de l'illite et les zones tout à fait supérieures du métamorphism. Etages Tectonique: 105-122.
- Limarino, C.O.; Spalletti, L.A. 2006. Paleogeography of the upper Paleozoic basins of southern South America: An overview. Journal of South American Earth Sciences 22: 134-155. doi:10.1016/j.jsames.2006.09.011.
- Löbens, S.; Bense, F.A.; Wemmer, K.; Dunkl, I.; Costa, C.H.; Layer, P.; Siegesmund, S. 2011. Exhumation and uplift of the Sierras Pampeanas: preliminary implications from K-Ar fault gouge dating and low-T thermochronology in the Sierra de Comechingones (Argentina). International Journal of Earth Sciences 100 (2-3): 671-694. doi:10.1007/s00531-010-0608-0.
- Löbens, S.; Sobel, E.R.; Bense, F.A.; Wemmer, K.; Dunkl, I.; Siegesmund, S. 2013a. Refined exhumation history of the northern Sierras Pampeanas, Argentina. Tectonics 32: 453-472.
- Löbens, S.; Bense, F.A.; Dunkl, I.; Wemmer, K.; Kley, J.; Siegesmund, S. 2013b. Thermochronological constraints of the exhumation and uplift of the Sierra de Pie de Palo, NW Argentina. Journal of South American Earth Sciences 48: 209-219.
- López, M.; Solá, P. 1981. Manifestaciones volcánicas alcalinas de los alrededores de Las Chacras y de la región de Villa Mercedes-Caján, provincia de San Luis y Córdoba. *In* Congreso Geológico Argentino, No. 8, Actas IV: 967-978. San Luis.
- Lyons, J.B.; Schnellenberg, J. 1971. Dating faults. Geological Society of America Bulletin 82: 1749-1752.
- Llambías, E.J.; Brogioni, N. 1981. Magmatismo mesozoico y cenozoico. *In* Geología y Recursos Naturales de la provincia de San Luis (Yrigoyen, M.; editor).
  Congreso Geológico Argentino, No. 8, Relatorio: 101-115. Buenos Aires.

- McDougall, I.; Harrison, T.M. 1999. Geochronology and Thermochronology by the <sup>40</sup>Ar/<sup>39</sup>Ar method, 2nd edition. Oxford University Press: 269 p. New York.
- McDowell, F.W.; McIntosh, W.C.; Farley, K.A. 2005. A precise 40 Ar/39 Ar reference age for the Durango apatite (U-Th)/He and fission-track dating standard. Chemical Geology 214 (3-4): 249-263.
- Maxwell, D.T.; Hower, J. 1967. High-grade diagenesis and low-grade metamorphism of illite in the Precambrian Belt Series. American Mineralogist 52: 843-857.
- Miller, H.; Söllner, F. 2005. The Famatina complex (NW Argentina): back-docking of an island arc or terrane accretion? Early Palaeozoic geodynamics at the western Gondwana margin. *In* Terrane processes at the margins of Gondwana (Vaughan, A.P.M.; Leat, P.T.; Pankhurst, R.J.; editors). Geological Society, Special Publications 246: 241-256. London.
- Morosini, A.; Ortiz Suárez, A.; Otamendi, J.; Pagano, D.; Ramos, G. 2017. La Escalerilla pluton, San Luis Argentina: The orogenic and post-orogenic magmatic evolution of the famatinian cycle at Sierras de San Luis. Journal of South American Earth Sciences 73: 100-118.
- Mpodozis, C.; Ramos, V.A. 1989. The Andes of Chile and Argentina. *In* Geology of the Andes and its relation to hydrocarbon and mineral resources (Ericksen, G.E.; Cañas Pinochet, M.T.; Rieinemud. J.A.; editors). Circumpacific Council for Energy and Mineral Resources, Earth Science Series 11: 59-90. Houston.
- Müller, M.J. 1996. Handbuch ausgewählter Klimastationen der Erde. Universität Trier: 346 p. Trier.
- Ortiz Suárez, A.; Prozzi, C.R.; Llambías, E.J. 1992. Geología de la parte sur de la Sierra de San Luis y granitoides asociados, Argentina. Estudios Geológicos 48: 269-277.
- Passchier, C.W.; Trouw, R.A.J. 2005. Microtectonics. Springer: 366 p. Berlín Heidelberg.
- Peacor, D.R.; Bauluz, B.; Dong, H.; Tillick, D.; Yan, Y. 2002. Transmission and analytical electron microscopy evidence for high Mg contents of 1M illite: absence of 1M polytypism in normal prograde diagenetic sequences of pelitic rocks. Clays and Clay Minerals 50 (2): 757-765.
- Purdy, J.; Jäger, E. 1976. K-Ar ages on rock-forming minerals from the Central Alps. Memorie dell' Instituto della Regia Università di Padova 30: 1-31.
- Rabassa, J.; Carignano, C.; Cioccale, M. 2010. Gondwana Paleosurfaces in Argentina: An introduction. Geociências 29 (4): 439-466.
- Rabassa, J.; Carignano, C.; Cioccale, M. 2014. A general overview of Gondwana landscapes in Argentina. *In*

- Gondwana Landscapes in southern South America, (Rabassa, J.; Ollier, C.; editors). Springer Earth System Sciences: 201-245. doi: 10.1007/978-94-007-7702-6 9.
- Ramos, V.A. 1988. The tectonics of the Central Andes: 30° to 33°S latitude. *In* Processes in continental lithospheric deformation (Clark, S.; Burchfiel, D.; editors). Geological Society of America, Special Paper 218: 31-54.
- Ramos, V.A. 2009. The Grenville-Age Basement of the Andes. Journal of South American Earth Sciences. doi: 10.1016/j.jsames.2009.09.004.
- Ramos, V.A.; Cristallini, E.; Pérez, D. 2002. The Pampean flat-slab of the central Andes. Journal of South American Earth Sciences 15: 59-78.
- Reynolds, R.C. Jr. 1963. Potassium~rubidium ratios and polytypism in illites and microclines from the clay size fractions of proterozoic carbonate rocks. Geochimica et Cosmochimica, Acta 27: 1097-1112.
- Reynolds, R.C. Jr.; Thomson C.H. 1993. Illite from the Potsdam sandstone of New York: A probable noncentrosymetric mica structure. Clays and Clay Minerals 41: 66-72.
- Reiners, P.W.; Brandon, M.T. 2006. Using Thermochronology to Understand Orogenic Erosion. Annual Review of Earth and Planetary Sciences 34: 419-466.
- Richardson, T.; Ridgway, K.D.; Gilbert, H.; Martino, R.; Enkelmann, E.; Anderson, M.; Alvarado, P. 2013. Neogene and Quaternary tectonics of the Eastern Sierras Pampeanas, Argentina: Active intraplate deformation inboard of flat-subduction. Tectonics 32: 780-796.
- Ring, U.; Brandon, M.T.; Willet, S.D.; Lister, G.S. 1999. Exhumation processes. *In* Exhumation processes: normal faulting, ductile flow and erosion (Ring, U.; Brandon, M.T.; Lister, G.S.; Willet, S.D.; editors). Geological Society, Special Publications 154: 1-27. London.
- Salfity, J.A.; Gorustovich, S.A. 1983. Paleogeografía del Grupo Paganzo (Paleozoico Superior). Revista de la Asociación Geológica Argentina 38: 437-453.
- Sato, A.; González, P.; Llambías, E. 2003. Evolución del orógeno Famatiniano en la Sierra de San Luis: magmatismo de arco, deformación y metamorfismo de bajo a alto grado. Revista de la Asociación Geológica Argentina 58: 487-504.
- Sato, A.M.; Llambías, E.J.; Basei, M.A.S.; Castro, C.E. 2015. Three stages in the Late Paleozoic to Triassic magmatism of southwestern Gondwana, and the relationships with the volcanogenic events in coeval basins. Journal of South American Earth Sciences 63: 48-69.
- Schmidt, C.J.; Astini, R.A.; Costa, C.H.; Gardini, C.E.; Kraemer, P.E. 1995. Cretaceous rifting, alluvial fan

- sedimentation, and Neogene inversion, southern Sierras Pampeanas, Argentina. *In* Petroleum Basins of South America (Tankard, A.J.; Suárez Soruco, R.; Welsink, H.J.; editors). American Association of Petroleum Geologists Memoir: 341-358.
- Schmitz, M.D.; Bowring, S. 2001. U-Pb zircon and titanite systematics of the Fish Canyon Tuff: an assessment of high-precision U-Pb geochronology and its application to young volcanic rocks. Geochimica et Cosmochimica Acta 65: 2571-2587.
- Schumacher, E. 1975. Herstellung von 99,9997% <sup>38</sup>Ar für die <sup>40</sup>K/<sup>40</sup>Ar Geochronologie. Geochronologia Chimica 24: 441-442.
- Siegesmund, S.; Steenken, A.; López de Luchi, M.G.; Wemmer, K.; Hoffmann, A.; Mosch, S. 2004. The Las Chacras-Potrerillos Batholith, Pampean Ranges, Argentina; structural evidences, emplacement and timing of the intrusion. International Journal of Earth Sciences 93 (1): 23-43.
- Sims, J.; Stuart-Smith, P.; Lyons, P.; Skirrow, R. 1997.
  1:250.000 Scale Geological and Metallogenetic Maps.
  Sierras de San Luis and Comechingones, Provinces of San Luis and Córdoba. Final report. Geoscientific Mapping of the Sierras Pampeanas Argentine-Australia Cooperative Project. Australian Geological Survey Organization. Servicio Geológico Minero Argentino (SEGEMAR): 123 p.
- Sims, J.P.; Ireland, T.R.; Camacho, A.; Lyons, E.; Pieters, P.E.; Skirrow, R.G.; Stuart-Smith, P.G.; Miró, R. 1998.
  U-Pb, Th-Pb and Ar/Ar geochronology from the southern Sierras Pampeanas, Argentina: implications for the Palaeozoic tectonic evolution of the western Gondwana margin. *In* The Proto-Andean Margin of Gondwana (Pankhurst, R.J.; Rapela, C.W.; editors). Geological Society, Special Publications142: 259-281. London.
- Solum, J.G.; van der Pluijm, B.A.; Peacor, D.R. 2005. Neocrystallization, fabrics and age of clay minerals from an exposure of the Moab Fault, Utah. Journal of Structural Geology 27 (9): 1563-1576.
- Środoń, J.; Eberl, D.D. 1984. Illite. Reviews in Mineralogy and Geochemistry 13 (1): 495-544.
- Surace, I.R.; Clauer, N.; Thélin, P.; Pfeifer, H. 2011. Structural analysis, clay mineralogy and K-Ar dating of fault gouges from Centovalli Line (Central Alps) for reconstruction of their recent activity. Tectonophysics 510 (1-2): 80-93.
- Steenken, A.; López de Luchi, M.G.; Siegesmund, S.; Wemmer, K.; Pawlig, S. 2004. Crustal provenance and cooling of basement complexes of the Sierra

- de San Luis: An insight into the tectonic history of the proto-Andean margin of Gondwana. Gondwana Research 7 (4): 1171-1195.
- Steenken, A.; Siegesmund, S.; Wemmer, K.; López de Luchi, M.G. 2008. Time constraints on the Famatinian and Achalian structural evolution of the basement of the Sierra de San Luis (Eastern Sierras Pampeanas, Argentina). Journal of South American Earth Sciences 25 (3): 336-358. doi:10.1016/j.jsames.2007.05.002.
- Steenken, A.; Wemmer, K.; Martino, R.D.; López de Luchi, M.G.; Guereschi, A.; Siegesmund, S. 2010. Post-Pampean cooling and the uplift of the Sierras Pampeanas in the west of Córdoba (Central Argentina). Neues Jahrbuch für Geologie und Paläontologie Abhandlungen 256: 235-255.
- Steiger, R.H.; Jaeger, E. 1977. Subcommission on geochronology; convention on the use of decay constants in geo- and cosmochronology. Earth and Planetary Science Letters 36 (3): 359-362.
- Stüwe, K.; Barr, T.D. 1998. On uplift and exhumation during convergence. Tectonics 17: 80-88.
- Velde, B. 1965. Experimental determination of muscovite polymorph stabilities. American Mineralogist 50: 436-449.
- Von Gosen, W. 1998. Transpressive deformation in the southwestern part of the Sierra de San Luis (Sierras Pampeanas, Argentina). Journal of South American Earth Sciences 11 (3): 233-264.
- Von Gosen, W.; Loske, W.; Prozzi, C. 2002. New isotopic dating of intrusive rocks in the Sierra de San Luis (Argentina): implications for the geodynamic history of the Eastern Sierras Pampeanas. Journal of South American Earth Sciences 15: 237-250.
- Weaver, C.E. 1989. Clays, muds and Shales. Developments in Sedimentology 44: 818 p. Elsevier, Amsterdam.
- Weber, K. 1972. Notes on the determination of illite crystallinity. Neues Jahrbuch für Geologie und Paläontologie Monatshefte 6: 267-276.
- Wemmer, K. 1991. K-Ar-Alterdatierungsmöglichkeiten für retrograde Deformationsprozesse im spröden und duktilen Bereich-Beispiele aus der KTB-Vorbohrung (Oberpfalz) und dem Bereich der Insubrischen Linie (N-Italien). Göttinger Arbeiten zur Geologie und Paläontologie 51: 1-61.
- Wemmer, K.; Ahrendt, H. 1997. Comparative K-Ar and Rb-Sr age determinations of retrograde processes on rocks from the KTB deep drilling project. Geologische Rundschau 86: 272-285.

- Wemmer, K.; Steenken, A.; Müller, S.; López de Luchi, M.G.; Siegesmund, S. 2011. The tectonic significance of K-Ar illite fine-fraction ages from the San Luis Formation (Eastern Sierras Pampeanas, Argentina). International Journal of Earth Sciences 100 (2-3): 659-669. doi:10.1007/s00531-010-0629-8.
- Whitmeyer, S.J. 2008. Dating fault fabrics using modern techniques of <sup>40</sup>Ar/<sup>39</sup>Ar thermochronology: evidence for Paleozoic deformation in the Eastern Sierras Pampeanas, Argentina. Journal of the Virtual Explorer 30, paper 3. doi: 10.3809/jvirtex.2008.00207.
- Willner, A.P.; Gerdes, A.; Massonne, H.-J.; Schmidt, A.; Sudo, M.; Thomson, S.N.; Vujovich, G. 2011. The geodynamics of collision of a microplate (Chilenia) in Devonian times deduced by the pressure-temperature-time evolution within part of a collisional belt (Guarguaraz Complex, W-Argentina). Contributions to Mineralogy and Petrology 162: 303-327.
- Wolf, R.A.; Farley, K.A.; Kass, D.M. 1998. Modeling of the temperature sensitivity of the apatite (U-Th)/He thermo-chronometer. Chemical Geology 148 (1-2): 105-114
- Wolff, R.; Dunkl, I.; Kiesselbach, G.; Wemmer, K.; Siegesmund, S. 2012. Thermochronological constraints on the multiphase exhumation history of the Ivrea-Verbano Zone of the Southern Alps. Tectonophysics 579: 104-117. doi:10.1016/j.tecto.2012.03.019.
- Yáñez, G.; Ranero, G.R.; von Huene, R.; Díaz, J. 2001. Magnetic anomaly interpretation across the southern central Andes (32°-34°S): The role of the Juan Fernández Ridge in the late Tertiary evolution of the margin. Journal of Geophysical Research 106: 6325-6345.
- Yoder, H.S.; Eugster, H.P. 1955. Synthetic and natural muscovite. Geochimica et Cosmochimica Acta 8: 225-280.
- Yrigoyen, M. 1975. La edad Cretácica del Grupo Gigante (San Luis), su relación con cuencas circunvecinas. *In* Congreso Geologico Argentino de Paleontología y Biostratigrafía, No. 1, Actas 2: 29-56. Tucumán.
- Zoeller, M.; Brockamp, O. 1997. 1M-and 2M (sub 1)illites; different minerals and not polytypes; results from single crystal investigations at the transmission electron microscope (TEM). European Journal of Mineralogy 9 (4): 821-827.
- Zwingmann, H.; Yamada, K.; Tagami, T. 2010. Timing of brittle deformation within the Nojima fault zone, Japan. Chemical Geology 275 (3-4): 176-185.

## **Appendix**

## (U-Th)/He analytical procedure

For this work 2-4 apatite single crystals aliquots from seven samples as well as three zircon single crystals aliquots from four samples were carefully hand-picked using binocular and petrologic microscope. Only inclusion and fissure-free grains showing a well-defined external morphology were used, whereas euhedral crystals were preferred. The shape parameters of each single crystal were determined, *e.g.*, length and width, and archived by digital microphotographs in order to apply the correction of alpha ejection described by Farley and Wolf (1996). Subsequently, the crystals were wrapped in an approximately 1x1 mm sized platinum capsule and analysed following a two-stage analytical procedure (Reiners and Brandon, 2006). This is characterised by (a) measuring the <sup>4</sup>He extraction, and (b) by analysing the <sup>238</sup>U, <sup>232</sup>Th and Sm content of the same crystal. During the first step, operated by HeLID automation software through a K8000/Poirot interface board, the Pt capsules were degassed in high vacuum by heating with an infrared diode laser. The extracted gas was purified using a SAES Ti-Zr getter at 450 °C and the inert noble gases as well as a minor amount of rest gases were measured by a Hiden triple-filter quadrupole mass spectrometer equipped with a positive ion counting detector. Re-extraction was performed for each sample to control the quantitative amount of extracted helium. During the He measurement, 240 readings of the mass spectrometer were recorded for every standard and sample.

After degassing, the samples were retrieved from the gas extraction line and spiked with calibrated  $^{230}$ Th und  $^{233}$ U solutions. Zircon crystals were dissolved in pressurized Teflon bombs using distilled 48% HF + 65% HNO $_3$  for five days at 220 °C. For apatite 2% HNO $_3$  was used. These spiked solutions were then analysed by istope dilution method using a Perkin Elmer Elan DRC II ICP-MS provided with an APEX micro flow nebuliser.

To process and evaluate the He signal as well as the data of the ICP-MS measurements the factory-made software of the mass spectrometer MASsoft and the freeware software PEPITA (Dunkl *et al.*, 2008), were used. Regarding the He latter evaluation, 40 to 70 readings of the ICP-MS were considered and individual outliers of the  $^{233}\text{U}/^{238}\text{U}$  as well as  $^{230}\text{Th}/^{233}\text{Th}$  ratios were tested and rejected according to the  $^{26}$  deviation criterion.

Finally, the raw (U-Th)/He ages of zircon and apatite were form-corrected (Ft correction) following Farley and Wolf (1996) and Hourigan *et al.* (2005). Replicate analyses of Durango apatite over the period of this study yielded a mean (U-Th)/He age of 30.4±1.7 Ma, which is in good agreement with the reference (U-Th)/He age of 31.12±1.01 Ma (McDowell *et al.*, 2005). Replicate analyses of the Fish Canyon zircon standard yielded a mean (U-Th)/He age of 28.0±1.6 Ma, which is also in good agreement with the reference Ar/Ar age of 27.9±1.01 Ma (Hurford and Hammerschmidt, 1985) and reference U-Pb-age of 28,479±0.029 Ma (Schmitz and Bowring, 2001).

#### AFT analytical procedure

Following standard density and magnetic mineral separation techniques, the apatite samples were mounted on a glass slide with epoxy. According to Donelick *et al.* (1999) the mounts were etched at 21 °C for 20 s using 5.50 M nitric acid after grinding and polishing procedures in order to reveal spontaneous tracks within the apatite crystals. The external detector method described by Gleadow (1981) was used, whereby low-uranium muscovite sheets (Goodfellow mica) represent the external detector for induced tracks. For age determination, the zeta calibration approach was adopted (Hurford and Green, 1983) and 25 good-quality grains per sample were randomly selected and dated. The fission track ages were calculated using the software TRACKKEY version 4.2 (Dunkl, 2002). Further, for all samples that had been dated ten Dpar measurements per grain were averaged to evaluate possible populations of different apatite compositions. Additionally, for track length analysis around 50-60 horizontal confined tracks of each sample were measured considering their angle to c-axis (Donelick *et al.*, 1999).

## K-Ar fault gouge: data acquisition

Each sampled fault gouge consists of approximately 250-1,000 g of fresh material. After careful selection, about 200 g of clay material was dispersed in distilled water and sieved <63 μm. The grain-size fractions <2 μm and 2-6 μm are gained from <63 μm fraction by differential settling in distilled water (Atterberg method following Stoke's law). Enrichment of the grain-size fraction <0.2 μm was accelerated by ultracentrifugation. For details the reader is referred to Wemmer (1991). Following the concentration of the different grain-size fractions, the samples were subjected to isotope measurements for dating and X-ray diffraction for determining the mineralogy, IC and PT.

The XRD analysis was done using a Phillips PW 1800 X-ray diffractometer. For the identification of the mineral content a step scan  $(0.020^{\circ}2\theta)$  was performed in the range from 4 to  $70^{\circ}2\theta$ . This was important to verify the existence of illite and to rule out the occurrence of any other potassium-bearing minerals. The mineral composition of all samples is shown in table 2.

For the determination of the IC "thin" texture compounds according to Weber (1972) were prepared using 1.5 to 2.5 mg/cm² sample material. The metamorphic grade of the samples has been inferred from the peak width at half-height of the 10 Å peak (Kübler, 1967) using a software algorithm developed at the University of Göttingen by Friedrich (1991), rewritten to FORTRAN by K. Ullemeyer (Geomar, Kiel) in 2005.

Digital measurement was carried out by a step scan with 301 points in a range of  $7-10^{\circ}2\theta$ , using a scan step of  $0.01^{\circ}2\theta$  and an integration time of 4 s per step and a receiving slit of 0.1 mm as well as an automatic divergence slit. The presence of mixed layer clays that may obliterate the 10 Å peak has been tested by duplicate determination of the material under air-dry and glycolated conditions. Results of the IC determination are shown in table 3.

To determine the polytypism of illite, powder compounds were prepared and scanned in 561 steps in a range of 16-44°2θ, using a scan step of 0.05°2θ and an integration time of 30 s per step. The allocation of peaks to the corresponding polytypes was done as suggested by Grathoff and Moore (1996) and Grathoff *et al.* (1998). The randomness of orientation for the powder sample preparation was checked using the Dollase factor (Dollase, 1986). We tried to quantify the amount of different polytypes by several methods as described by Reynolds (1963); Maxwell and Hower (1967); Caillère *et al.* (1982); Grathoff and Moore (1996) and Grathoff *et al.* (1998), but due to bad peak shapes none of the used methods yield reasonable results. For this reason the general abundance of the polytypes was estimated as suggested by Grathoff and Moore (1996). The abundance of different polytypes in the analysed samples is shown in table 3.

Potassium and argon were determined following two different procedures. The argon isotopic composition was measured in a Pyrex glass extraction and purification vacuum line serviced with an on line <sup>38</sup>Ar spike pipette and coupled to a VG 1200 C noble gas mass spectrometer operating in static mode. Samples were pre-heated under vacuum at 120 °C for 24 h to reduce the amount of atmospheric argon adsorbed onto the mineral surfaces during sample preparation. Argon was extracted from the mineral fractions by fusing samples using a low blank resistance furnace within the Pyrex glass extraction and purification line.

The amount of radiogenic <sup>40</sup>Ar was determined by isotope dilution method using a highly enriched <sup>38</sup>Ar spike (Schumacher, 1975), which was calibrated against the biotite standard HD-B1 (Fuhrmann *et al.*, 1987; Hess and Lippolt, 1994). The released gases were subjected to a two-stage purification procedure via Tigetters and SORB-ACs getters. Blanks for the extraction line and mass spectrometer were systematically determined and the mass discrimination factor was monitored by airshots. The overall error of the argon analysis is below 1.00%. Potassium was determined in duplicate by flame photometry using an Eppendorf Elex 63/61. The samples were dissolved in a mixture of HF and HNO<sub>3</sub>. CsCl and LiCl were added as an ionisation buffer and internal standard, respectively. The pooled error of duplicate Potassium determination on samples and standards is better than 1%.

The K-Ar age were calculated based on the  $^{40}$ K abundance and decay constants recommended by the IUGS quoted in Steiger and Jäger (1977). The analytical error for the K-Ar age calculations is given at a 95% confidence level (2 $\sigma$ ). Analytical results are presented in table 3. Details of argon and potassium analyses for the laboratory in Göttingen are given in Wemmer (1991).

## K-Ar fault gouge data interpretation

One problem in dating fault gouge illites is the possible mixture of several illite generations, *i.e.*, illite may form by different events at different times. In the case of fault gouges developed from non-sedimentary host rock and cooled under retrograde conditions, illite can be assumed authigenic and neoformed and, thus, the finest illite fraction should represent the most recently grown illite. Coarser grain-size fraction should yield older ages, representing earlier illite-forming events (*e.g.*, Clauer *et al.*, 1997). However, illite grain-size fraction ages may not represent single geological events but an integration of events.

Available information on the effective diffusion radius and the closure temperature for the Ar-system in illite fine-fractions (grain size smaller than 2  $\mu$ m) is scarce but can be placed somewhere between 230 and 290 °C (Hunziker *et al.*, 1986; Wemmer and Ahrendt, 1997).

In addition to its age, the crystallinity of illite (IC, expressed as Kübler Index KI) and its polytypism can provide important constraints for the assessment of thermal evolution and very low metamorphism grades of fault gouges and their host rock. The illite crystallinity is defined after Kübler (1964) as the half-height width of the 10 Å XRD peak. The values for the illite crystallinity may range from  $0.060~\Delta^{\circ}2\theta$  for ideally ordered muscovite up to  $1~\Delta^{\circ}2\theta$  for illite/smectite mixed layers (Kübler, 1964). Kübler (1967) divided the zones of the very low-grade metamorphism into, from lower to higher grade, diagenetic zone (IC >0.420°2 $\theta$ ), anchizone (0.420°2 $\theta$  < IC >0.250°2 $\theta$ ) and epizone (IC <0.250°2 $\theta$ ), with corresponding temperature boundaries of around 150 °C and 300 °C, respectively (Fig. 4; Gharrabi *et al.*, 1998; Jaboyedoff *et al.*, 2000, 2001).

It is important to consider that the analysed grain-size fractions represent mixtures of illite formed at different time and temperature conditions, thus yielding different IC and polytypism. However, the KI values of authigenic fault gouge illite, even of mixtures, can be used to estimate the minimum temperature experienced by the fault gouge sample (Fig. 4). Additionally, KI values may help to decipher evolutionary differences between grain-size fractions within one sample as well as between samples.

Polytypism is a common phenomenon for layered silicate minerals. For illite, the most common polytypes are the 1M<sub>4</sub>, 1M and 2M<sub>1</sub> (e.g., Reynolds and Thomson, 1993). With increasing temperature, illite shows irreversible polytype transformation of the  $1M_d \rightarrow 1M \rightarrow 2M_1$  (Hunziker *et al.*, 1986). Yoder and Eugster (1955) and Weaver (1989) concluded that the transition from 1M<sub>d</sub> and 1M to 2M<sub>1</sub> begins at a temperature of approximately 200-210 °C (Fig. 4). Generally, illite has 1M<sub>a</sub> and 1M polytypes in the diagenetic zone, a mixture of 1M and 2M, polytypes in the anchizone and almost sole 2M, polytypes in the epizone (Fig. 4; e.g., Bailey, 1966; Środoń and Eberl, 1984). Using XRD patterns derived from randomly oriented samples, it is possible to quantify the relative amounts of 2M<sub>1</sub>, 1M and 1M<sub>d</sub> illite using a method proposed by Grathoff and Moore (1996). In literature dealing with dating of fault gouge from sedimentary rocks, the 1M<sub>d</sub> and 1M polytypes are generally considered authigenic products formed under diagenetic to anchimetamorphic, prograde conditions during subsequent burial and diagenesis of the host rock (e.g., Grathoff and Moore 1996). In contrast, due to its restriction to epizonal conditions, the 2M<sub>1</sub> illite polytype is considered a detrital component derived from source rock. Even when dealing with non-sedimentary host-rocks, the 2M<sub>1</sub> illite is excluded from consideration because temperature conditions in fault zone are regarded as insufficient for the development of 2M<sub>1</sub> illite (Fig. 13). However, Bense et al. (2014) conclude that, at higher temperatures, even 2M, illite could be developed in fault gouges, especially when fault gouge development took place at or directly after cooling of the host rock to brittle deformation temperatures (about 300 °C for quartz, e.g., Passchier and Trouw, 2005, and references therein). Thus, in contrast to sedimentary rocks, the development of 2M, illite polytypes in a brittle fault gouge must not be excluded from consideration when the host rock passed epizonal conditions during retrograde metamorphism due to regional cooling (Fig. 13).